Modelling the Electrical Activity of Pancreatic Beta Cells

Yosman BapatDhar

A dissertation submitted for the partial fulfilment of BS-MS Dual Degree in Science

Indian Institute of Science Education and Research, Mohali
April 2016

Certificate of Examination

This is to certify that the dissertation titled **"Modelling the Electrical Activity of Pancreatic Beta Cells"** submitted by **Ms. Yosman BapatDhar** (Reg. No. MS11060) for the partial fulfillment of BS-MS dual degree programme of the Institute, has been examined by the thesis committee duly appointed by the Institute. The committee finds the work done by the candidate satisfactory and recommends that the report be accepted.

Dr. Kavita Babu Dr. Shashi Bhushan Pandit Prof. Somdatta Sinha
(Supervisor)

Dated: April 22nd, 2016

Declaration

The work presented in this dissertation has been carried out by me under the guidance of Prof. Somdatta Sinha at the Indian Institute of Science Education and Research Mohali.

This work has not been submitted in part or in full for a degree, a diploma, or a fellowship to any other university or institute. Whenever contributions of others are involved, every effort is made to indicate this clearly, with due acknowledgment of collaborative research and discussions. This thesis is a bona-fide record of original work done by me and all sources listed within have been detailed in the bibliography.

Yosman BapatDhar

(Candidate)

Dated: April 22nd, 2016

In my capacity as the supervisor of the candidate's project work, I certify that the above statements by the candidate are true to the best of my knowledge.

Prof. Somdatta Sinha

(Supervisor)

Acknowledgements

My sincere gratitude to Prof. Somdatta Sinha, my research supervisor, for her patient guidance, useful critiques of the work and assistance in keeping my progress on schedule.

I thank all the members of the Computational and Mathematical Biology Group for their inputs during discussion sessions. I would like to specially acknowledge Vivek Sagar's help in troubleshooting some of my programs.

Finally, a huge thank you to my family and all my friends for keeping me sane and smiling throughout the year.

Abstract

The aim of this thesis project was to study the evolution of single cell mathematical models of the elctrical activity of pancreatic beta cells, find a candidate model that best matched experimental data present in the existing literature, and to use it to model gap-junction coupled beta cells present in pancreatic islets. This study found that the Dual Oscillator Model is currently the best model for the electrical activity of a single beta cell. It was found that the behaviour of a 1D ring of cells with nearest neighbour coupling depends upon the number of cells in the ring, the percentage composition of each of the cell types and the coupling strength (g_c) between neighbouring cells. Also, when multiple cells are coupled, synchronization of the burst goes from 180° anti phase (low g_c) to out of phase (intermediate g_c) to in phase (high g_c).

Contents

List of Figures

Chapter 1

Introduction

1.1 Electrically Active Cells

Electrically active cells are those cells that respond to changes in their membrane potential. Typically, their primary functions are regulated by changes in their membrane potential which occurs due to regulation of ionic fluxes. Examples are – neurons and conduction of action potentials; the electrical activity of cardiac cells for proper beating of the heart. Pancreatic beta cells are another example of electrically active cells. These cells respond to changes in their membrane voltage by secreting insulin.

1.1.1 Pancreatic *Islets of Langerhans*

Beta cells are specialized cells present in large numbers in structures called *Islets of Langerhans (Fig. 1.1)* in the Pancreas. Each islet consists of thousands of cells. In an islet thousands of beta cells generally form the core, and other cells (delta and alpha cells secreting glucagon and somatostatin hormones respectively) are present in the periphery *(Fig. 1.1).*

Beta cells respond to elevated blood glucose levels by secreting the hormone Insulin in a pulsatile manner[1,2]. Coordinated membrane voltage bursting in beta cells

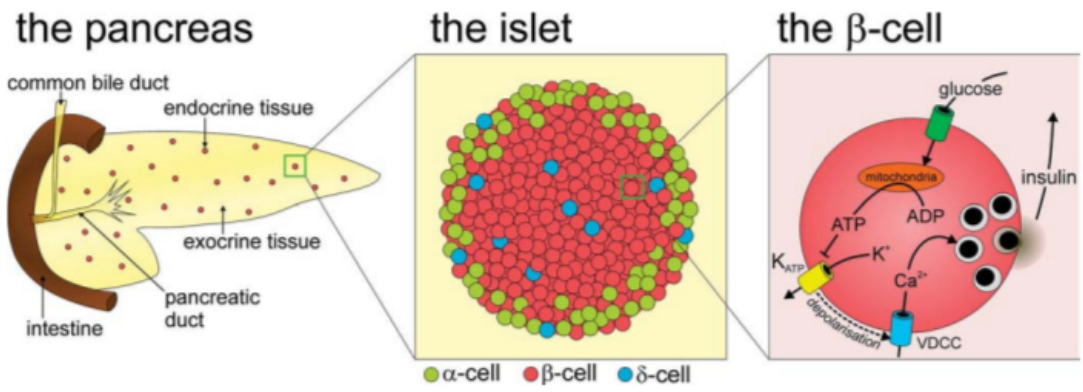

Figure 1.1: *The Pancreas, an Islet and a Beta Cell [9]*

(in an islet) *(Fig. 1.2)* precedes the rhythmic insulin secretion, and malfunction in the electrical activity of beta cells can lead to improper insulin secretion - a cause of Type 2 Diabetes[3]. Beta cells communicate (electrically) through membrane gap junctions (Connexin proteins). The major gap junction protein found between beta cells is Connexin-36 [6,7,8].

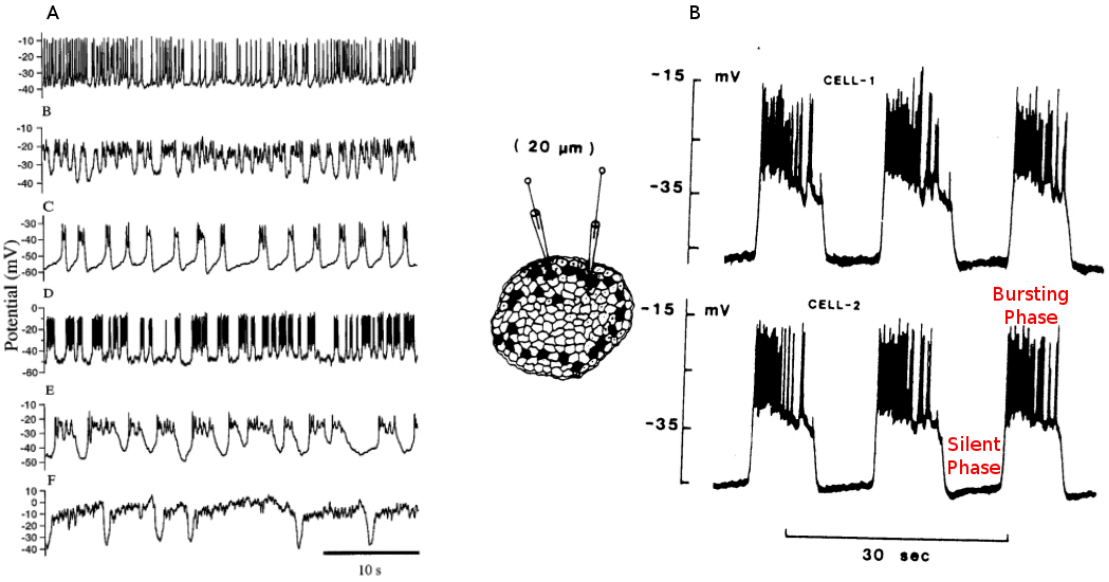

Figure 1.2: ***(A)*** *Voltage time curves for single beta cells* ***(B)*** *Voltage time curves of 2 coupled cells in the islet [11]*

Beta cell bursting consists of two phases: (1) A 'Silent' phase where the membrane voltage is approximately equal to the resting membrane voltage and (2) a 'Bursting' or an 'Active' phase where the membrane voltage fluctuates up and down rapidly *(Fig. 1.2 (B))*. The primary ionic currents responsible for membrane potential changes in beta cells are calcium and potassium currents of different types. Due to its involvement in diabetes, electrophysiological and pharmacological experiments and mathematical modelling of beta cell dynamics have been active areas of research.

1.2 Modelling the Biological Cell as an Electrical Circuit

The membrane of a biological cell provides a boundary separating the external environment from the internal environment of the cell *(Fig. 1.3(a))*. Typically, the membrane is selectively permeable thus regulating the passage of materials in and out of the cell. The cell membrane consists of a lipid bilayer (water insoluble) through which, irregularly interspersed, are globular proteins. The membrane also consists of protein lined water pores - channel proteins. Channel proteins (like voltage dependent calcium channels, VDCCs, ATP dependent potassium channels, K_{ATP} etc.) allow the passage of specific kinds of molecules. The selective permeability of the cell membrane and the presence of channel proteins results in a concentration difference across the membrane of various ions (Na^+, K^+, Ca^{+2}, Cl^-). These concentration differences are set-up and maintained by active processes that use ATP to pump ions against their electrochemical gradients.

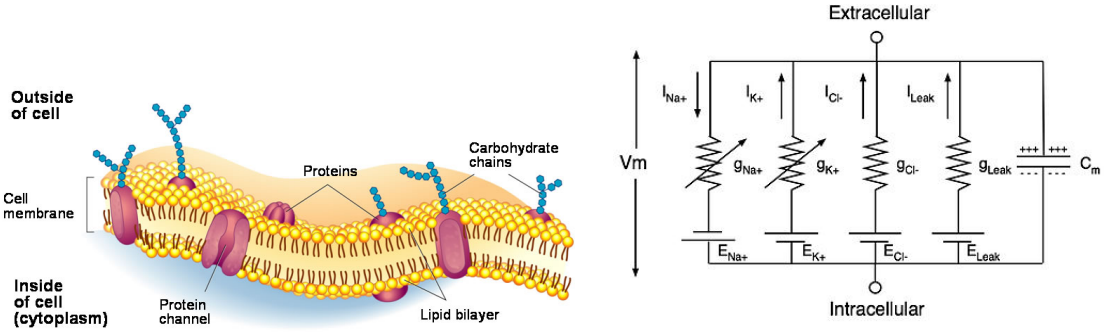

(a) The cell membrane [4]

(b) Equivalent electrical circuit of a cell membrane [5]

Figure 1.3: *The biological cell membrane as an electrical circuit*

Since the cell membrane separates and maintains a charge difference, it can be thought of as a capacitor *(Fig. 1.3(b))*. By the definition of the capacitance of a capacitor (ratio of charge across the capacitor to the voltage necessary to hold that charge), one can write: $C_m = \frac{Q}{V}$

Since current is defined as $\frac{dQ}{dt}$, it follows that the capacitative current is (assuming $C_m$to be constant):

$$C_m \frac{dV}{dt} \tag{1.1}$$

For a given ionic species, say Na^+, the potential drop across the cell membrane has two components: first due to concentration differences, given by the Nernst equation ($V_{Na} = \frac{RT}{ZF} \ln(\frac{[Na^+]_{external}}{[Na^+]_{internal}})$ and, second, due to an electrical current rI_{Na}(if the channel is Ohmic), where r is the resistance of the channel. Summing the two contributions

we get:

$$V = rI_{Na} + V_{Na} \tag{1.2}$$

Solving for current we get: $I_{Na} = g_{Na}(V - V_{Na})$ where $g_{Na} = \frac{1}{r}$ is the channel conductance.

Since there is no net build-up of charge on either side of a cell's membrane, the sum of the ionic and capacitative charges should be zero. Hence:

$$C_m \frac{dV}{dt} + I_{ionic} = 0 \tag{1.3}$$

1.2.1 The Hodgkin-Huxley Model (1952)

In 1952, Alan Hodgkin and Andrew Huxley published their Nobel prize winning work as a final paper [11] in a series of papers. This last paper is a landmark in the field of mathematical physiology. In this paper, Hodgkin and Huxley (HH) present elegant experimental data, a theoretical hypothesis, a fit of the model to the data and, most crucially, a testable prediction. This work stands out as a rare example of a successful combination of experiment and theory!

HH developed the first model of the propagation of an electrical signal along the axon of a nerve in the giant squid. This work is so important because, even though they originally used it to explain the propagation of electrical signals in a nerve cell, it has since then been extended and applied to model a wide variety of electrically excitable cells. The model (and equations) they proposed is mentioned, in brief, below.

In the previous section we described how the cell membrane could be modelled as a capacitor, resulting in the following equation:

$$C_m \frac{dV}{dt} + I_{ionic}(V,t) = 0 \tag{1.4}$$

In the giant squid axon, the main ionic currents are the sodium and potassium currents. HH lumped together the other, less significant, ion currents into one current called the *leak current (I_L).* HH assumed the membrane channel conductances to have linear I-V curves (this choice was largely dictated by experimental data) and so, we get:

$$C_m \frac{dV}{dt} = -g_{Na}(V - V_{Na}) - g_K(V - V_K) - g_L(V - V_L) \tag{1.5}$$

An important point to note is that the channel conductances are not constant; they seem to depend on the membrane voltage. Determining the conductances by being able to measure individual ionic currents and thus deducing the changes in conductances (with V) was what was brilliantly accomplished by Hodgkin and Huxley. They found, by performing various voltage clamp and space clamp experiments, that:

For the potassium current:

$$g_K = \bar{g}_k n^4$$

$$\frac{dn}{dt} = \alpha_n(1-n) - \beta_n n \qquad (1.6)$$

where n is an *activating* variable.

For the Sodium current:

$$g_{Na} = \bar{g}_{Na} m^3 h$$

$$\frac{dm}{dt} = \alpha_m(1-m) - \beta_m m \qquad (1.7)$$

$$\frac{dh}{dt} = \alpha_h(1-h) - \beta_h h \qquad (1.8)$$

where m is an *activating* variable and h is an *inactivating* variable.

The specific forms of α:

$$\alpha_m = 0.1\frac{25-V}{e^{(\frac{25-V}{10})}-1}$$

$$\alpha_h = 0.07e^{(\frac{-v}{20})}$$

$$\alpha_n = 0.01\frac{10-V}{e^{(\frac{10-v}{10})}-1}$$

The specific forms of β:

$$\beta_m = 4e^{(\frac{-V}{18})}$$

$$\beta_h = \frac{1}{e^{(\frac{30-V}{10})}+1}$$

$$\beta_n = 0.125e^{(\frac{-V}{18})}$$

Equations *1.5, 1.6, 1.7 and 1.8* are the four main equations, which, along with the functional forms of the activating/inactivating variables make up the HH model.

All the models describing the electrical activity of beta cells are based on the HH equations.

1.3 Glucose Stimulated Insulin Secretion (GSIS) in Beta Cells

Pancreatic beta cells synthesize and secrete the hormone insulin, the only known hormone responsible for lowering blood glucose levels. Under normal conditions, insulin is secreted in a pulsatile manner [1,2]. Interestingly, insulin oscillations are disrupted in patients with Type 2 diabetes[3]. In beta cells, glucose stimulated insulin secretion (GSIS) is driven by a well established sequence of events *(Fig. 1.4)*.

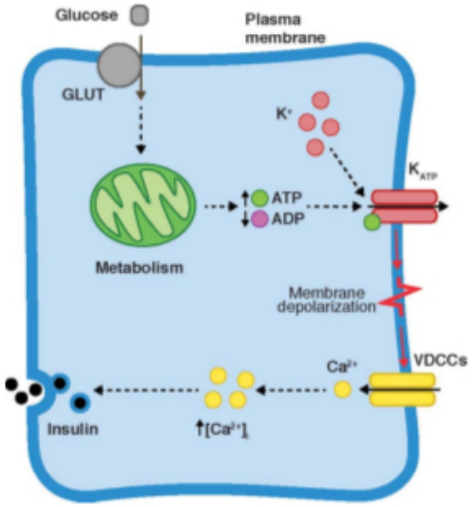

Glucose is metabolized after it is transported into the cell by GLUT transporters. This triggers the production of ATP and the subsequent closure of K_{ATP} channels. The membrane gets depolarized and VDCCs open, allowing an influx of Ca^{+2} ions. The increase in $[Ca^{+2}]_i$ stimulates insulin secretion in a Ca^{+2} - dependent manner.

Figure 1.4: *Schematic of GSIS in beta cells*

GSIS begins with the transport of glucose into the cell through glucose transporters (GLUT). The increased intracellular concentration of glucose accelerates metabolism and hence, the production of ATP at the expense of ADP. This results in an increase in the ATP/ADP ratio, causing the inactivation of ATP dependent Potassium channels (K_{ATP}), resulting in the slow depolarization of the membrane potential. Once the membrane potential crosses a threshold value, Voltage Dependent Calcium Channels (VDCCs) open and Ca^{+2} enters the cell. It is this increase in $[Ca^{+2}]_i$ that cause insulin secretion. This is the main pathway of GSIS (also called the triggering or K_{ATP}-dependent pathway).

As a complement to experimental work, mathematical models of beta cells have been built to better understand how various cellular mechanisms involved in GSIS interact and to provide feasible explanations of experimental observations and predictions. As more and more experimental evidence has emerged, models have grown in complexity: from the early, minimal model that just included a few ion channels, to models that incorporate detailed representations of metabolism, glycolysis and electrical activity.

1.4 Aim and Organization of the Thesis

The aim of this study is, broadly, to understand how mathematical models are formulated based on experimental information; how models are improved by incorporating new experimental information; how computational techniques can be used to mimic experimental manipulations and study the resultant behaviour of the theoretical model; and finally, to offer new theoretical predictions that can be tested experimentally. Specifically, I have used Pancreatic beta cells as my model.

In chapter 2 all the single cell models and methods used have been described.

In chapter 3 the simulation results of the electrical activity of the single cell models, two coupled cells and multiple coupled cells have been presented.

In chapter 4 a summary of the results and possible future directions the work in this thesis can be extended to have been mentioned.

In chapter 5 the literature referred to in this thesis has been listed chapter-wise.

All the MATLAB codes used have been attached in Appendix A.

Chapter 2

Models and Methods

2.1 Models

Mathematical models of beta cells have been proposed as tools to describe how various cellular processes interact in GSIS. As models have evolved over time, more and more of the cellular processes (described in the previous section) have been included in models of beta cells.

The pioneering model was published in 1983 by Chay and Keizer [1]. This model builds on the Hodgkin-Huxley paradigm [2]. The first models (Chay-Keizer[1], Chay[13]) explained fast bursting of membrane potential correctly but predicted oscillations of cytosolic [Ca^{+2}] with different kinetics than what was seen experimentally. With the discovery of ATP dependent Potassium Channels (K_{ATP})[4,5] in 1984, a set of models including K_{ATP} channels came up (Keizer and Magnus[11,12], Smolen and Keizer[6]). In order to explain the origins of extremely slow bursting (period of many minutes)[15,16,17], a wave of models in which the ER was included as a second Ca^{+2} compartment came up (Bertram *et. al.*[18], Chay *et.al.*[19]). Some other scientists have proposed an alternative mechanism to explain the wide range in the periodicity of bursting - the idea that the periodicity is based on the interactions between a fast and a slow variable(s) (Bertram *et. al.*[7], Bertram and Sherman[8], Bertram *et. al.*[9]). The current generation of models can explain the full range of observed bursting periods.

All the models mentioned so far (and the ones described in the next sections) are based on rodent experimental data. Human pancreatic beta cells differ from rodent beta cells in a few ways (distribution of cells in the islet[20], the types of ion channels expressed[21,22] and kinetics of insulin exocytosis[23]). Based on these differences (and based on the existing rodent models), mathematical models of human beta cells are currently in the early stages of development.

In this section four of the models based on rodent beta cells are described - mathematically and in terms of the physiological mechanisms involved.

2.1.1 Chay-Keizer Model (1983)

Chay and Keizer [1] (CK) developed their pioneering model of the beta cell in 1983. A schematic of the CK model is shown in figure 2.1. The ion channels they considered are: Voltage Dependent Calcium Channels (VDCCs), Voltage Dependent Potassium Channels (K_V) and Calcium Dependent Potassium Channels (K_{Ca}). The form of the equations used to describe the ion channels is the HH type[2]. Intracellular calcium handling is modelled in a minimal manner. As proposed by Atwater et. al. [3], the CK model uses the effects of intracellular calcium concentrations ($[Ca^{+2}]_i$) on K_{Ca}channels as the mechanism to terminate or initiate bursts of potential.

The active phase, shown by (1) in figure 2.1, is sustained by K_V and VDCCs and $[Ca^{+2}]_i$ slowly rises. Eventually, the K_{Ca}channels get activated and the membrane repolarizes (shown by (2)). During the silent phase (shown by (3)), the VDCCs and K_V channels are closed and $[Ca^{+2}]_i$ is extruded from the cell, inhibiting the activity of the K_{Ca}channels. This causes depolarization of the membrane potential, activating the VDCCs and K_V channels, initiating a new burst.

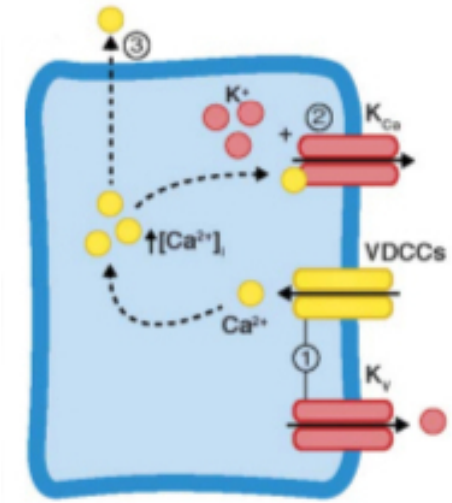

Figure 2.1: *Schematic of the Chay-Keizer Model [14]*

The Model Equations

The differential equations:

$$\frac{dV}{dt} = \frac{1}{C_m}(2I_{Ca} + I_K + I_{KCa} + I_l)$$

$$\frac{dm_{Ca}}{dt} = \phi\,(\alpha_{mCa}(1 - m_{Ca}) + \beta_{mCa}m_{Ca})$$

$$\frac{dh_{Ca}}{dt} = \phi\,(\alpha_{hCa}(1 - h_{Ca}) + \beta_{hCa}h_{Ca})$$

$$\frac{dn}{dt} = \phi\,(\alpha_n(1 - n) + \beta_n n)$$

$$\frac{dCa}{dt} = f\left(\frac{3}{r}I_{Ca} - K_{Ca}Ca\right)$$

The ionic currents:

$$I_{Ca} = g_{Ca}m_{Ca}^3 h_{Ca}(V_{Ca} - V)$$

$$I_K = g_K n^4 (V_K - V)$$

$$I_{KCa} = g_{KCa}\frac{Ca}{Ca + K_{diss}}(V_K - V)$$

$$I_l = g_l(V_l - V)$$

Parameter	Value
$C_m(\mu F/cm^2)$	1
$g_{Ca}(mS/cm^2)$	6.5
$g_K(mS/cm^2)$	12
$g_l(mS/cm^2)$	0.04
$g_{KCa}(mS/cm^2)$	0.09
$V_{Ca}(mV)$	100
$V_K(mV)$	−75
$V_l(mV)$	−40
$V'(mV)$	50
$V^*(mV)$	30
$T(^0C)$	20
$r(\mu m)$	8.9×10^{-4}
f	0.004
$K_{diss}(\mu M)$	1
$K_{Ca}(\mu M)$	0.04

Gating functions:

$$\alpha_{mCa} = -0.1 \frac{(V+V'-25)}{e^{-\frac{(V+V'-25)}{10}}-1}$$

$$\beta_{mCa} = 4e^{-\frac{(V+V')}{18}}$$

$$\alpha_{hCa} = 0.07e^{-\frac{(V+V')}{20}}$$

$$\beta_{hCa} = \frac{1}{e^{-\frac{(V+V')-30}{10}}+1}$$

$$\alpha_n = -0.01 \frac{(V+V^*-10)}{e^{-\frac{V+V^*-10}{10}}-1}$$

$$\beta_n = 0.125e^{-\frac{V+V^*}{80}}$$

$$\phi = 3^{\frac{T-6.3}{10}}$$

2.1.2 Smolen-Keizer Model (1992)

In 1984 ATP dependent Potassium Channels (K_{ATP}) were identified in rodent beta cells [4,5], emerging as a probably link between metabolism and electrical activity. The activity of K_{ATP} channels is inhibited by ATP and stimulated by ADP. These channels are responsible for the resting membrane potential of beta cells. Smolen and Keizer [6] (SK) introduced K_{ATP} channels to the models of beta cells in order to analyze the role of cyclical changes in the ATP/ADP ratio on the electrical activity of beta cells. This model assumes as negative influence of Ca^{+2} on the production of ATP. A schematic of the SK model is shown in figure 2.2.

The active phase, shown by (1) in figure 2.2, is sustained by K_V and VDCCs and $[Ca^{+2}]_i$ slowly rises. This exerts a negative effect on the production of ATP (reflected in the increase of ADP) causing a corresponding decrease in the ATP/ADP ratio. As a consequence, K_{ATP} channels open, repolarizing the membrane (shown by (2)). During the silent phase (shown by (3)), the K_V channels and VDCCs are closed and $[Ca^{+2}]_i$is extruded from the cell. As $[Ca^{+2}]_i$ decreases, the production of ATP is

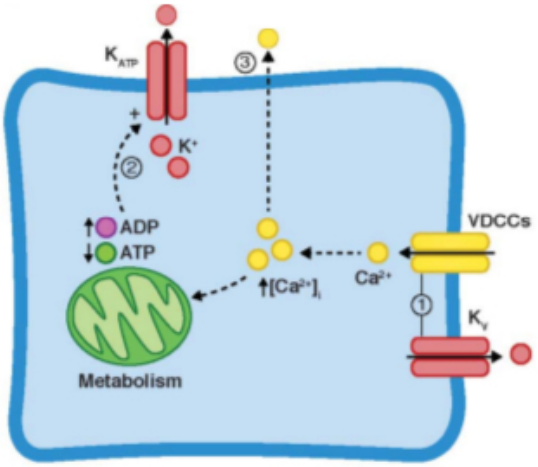

Figure 2.2: *Schematic of the Smolen-Keizer Model [14]*

potentiated, closing the K_{ATP} channels and initiating a slow depolarization of the membrane, initiating a new cycle.

The Model Equations

The differential equations: **The ionic currents:**

$$\frac{dV}{dt} = -\frac{1}{C_m}(I_{Ca} + I_K + I_{KATP}) \qquad I_{Ca} = g_{Cab} g_{hk}$$

$$\frac{dn}{dt} = \lambda_a(\phi_k - n)\frac{1}{\tau_n} \qquad I_{KV} = g_k \cdot ii \cdot n(V - V_K)$$

$$\frac{dCa}{dt} = f \cdot (\alpha I_{Ca} - a_{kca} Ca - \frac{d_{amp} ca^{hill}}{a_{kdamp}^{hill} + ca^{hill}} \qquad I_{KATP} = g_{ATP}(V - V_K)$$

$$\frac{dd}{dt} = k_a((tot - d) - d$$

$$\frac{dpc}{dt} = k_{1p} pot(1 - f_{2\infty}) - k_{1m} pc$$

$$\frac{dpot}{dt} = -(k_{1p} pot \cdot (1 - f_{2\infty}) - k_{1m} pc - \lambda_k(k_{3p} \cdot f_{2\infty} \cdot pot - k_{3m}(1 - pot \cdot pc))$$

$$\frac{dii}{dt} = \lambda_i \frac{(\phi_i - ii)}{\tau_i}$$

$$\frac{djj}{dt} = \lambda_j \frac{(\phi_j - jj)}{\tau_j}$$

Other equations:

Paramater	Values	Parameter	Values
V_K (mV)	-75	g_{cam} (pS)	1470
C_m (μF/cm^2)	5309	χ	0.27
V_{mj} (mV)	-11	S_{mj} (mV)	3.6
g_{cal} (pS)	6.3	Ca_0(mM)	7
g_K (pS)	5000	$\bar{g}_{ATP}$ (pS)	6000
K_1 (μM)	0.45	K_2 (μM)	0.012
V_n (mV)	-20	λ_a	1.2
S_n (mV)	5.3	f	0.03
k_a(ms^{-1})	2×10^{-5}	$r(\mu$m)	0.76
$r_1(\mu$m)	0.35	λ_m	0.78
V_m(mV)	-15	S_m(mV)	6.2
k_{2s}(ms^{-1})	1.512	k_{2m}(ms^{-1})	65
λ_K	1	k_{3p}(ms^{-1})	0.02
λ_i	1	V_i (mV)	36
S_i (mV)	4.5	τ_i(ms)	2600
λ_j	1	V_j	50
S_j(mV)	6.3	τ_j(ms)	50000

$$\phi_{CaJ} = \frac{1}{1+e^{\frac{V_{mj}-V}{S_{mj}}}}$$

$$\phi_K = \frac{1}{1+e^{\frac{V_n-V}{S_n}}}$$

$$\phi_{Ca} = \frac{1}{1+e^{\frac{V_m-V}{S_m}}}$$

$$\phi_i = \frac{1}{1+e^{\frac{V_i+V}{S_i}}}$$

$$\phi_j = \frac{1}{1+e^{\frac{V_j+V}{S_j}}}$$

$$k_{1m} = \lambda_m \phi_{ICa}$$

$$k_{1p} = \lambda_m(1-\phi_{ICa})$$

$$k_{2p} = -k_{2s} g_{hk}$$

$$g_{Cab} = g_{Cam}(\chi P + (1-\chi)\phi_{CaJ} jj) + g_{Cal}$$

$$g_{hk} = \frac{Ca_0 V}{1-e^{\frac{V}{13.35}}}$$

$$g_{ATP} = \bar{g}_{ATP}\frac{1+\frac{d}{k_1}}{1+\frac{d}{k_1}+\frac{tot-d}{k_2}}$$

$$f_{2\infty} = \frac{k_{2p}}{k_{2m}+k_{2p}}$$

$$\alpha = \frac{3000}{8\pi(96487)7^3}$$

$$\alpha_n = e^{\frac{V+75}{65}}$$

$$\beta_n = e^{\frac{V+75}{65}}$$

$$\tau_n = \frac{60}{\alpha_n+\beta_n}$$

$$\tau_j = \tau_{jmin} + \frac{\tau_j}{e^{\frac{V+V_j}{2S_j}}+e^{-\frac{V+V_j}{2S_j}}}$$

2.1.3 Phantom Burster Model (2000)

Bertram *et. al.*[7] developed a model based on the idea that the periodicity of bursting is determined by the interaction between a fast and a slowly oscillating variable. This model is capable of producing bursting with an intermediate period, distinct from that of the fast and the slow variables. Hence, models of this type are called phantom bursters. s1 is the faster variable and s2 the slower one. For the purposes of the model it is sufficient if I_{s1} and I_{s2} are repolarizing, negative feedback currents that turn on

when the cell is depolarized (Alternatively, they could be depolarizing currents that turn off when the cell is depolarized). There are many candidates for the identity of the fast and slow processes - their exact biophysical identities remain obscure. Bertram *et. al.*[7] suggest that I_{s1} could be though of as a current through K_{Ca} channels and I_{s2} as a current though K_{ATP} channels. Notice that neither of these channels is directly voltage dependent but both channels respond to changes in $[Ca^{+2}]_i$ levels which is voltage dependent.

The Model Equations

The differential equations:

$$\frac{dV}{dt} = -\frac{1}{C_m}\left(I_{Ca} + I_K + I_l + I_{s1} + I_{s2} + I_{\text{stim}}\right)$$

$$\frac{dn}{dt} = \lambda \frac{n_\infty - n}{\tau_n}$$

$$\frac{ds_1}{dt} = \frac{s_{1\infty} - s_1}{\tau_{s1}}$$

$$\frac{ds_2}{dt} = \frac{s_{2\infty} - s_2}{\tau_{s2}}$$

The ionic currents:

$$I_{Ca} = g_{Ca} m_\infty (V - V_{Ca})$$

$$I_K = g_K n (V - V_K)$$

$$I_l = g_l (V - V_l)$$

$$I_{s1} = g_{s1} s_1 (V - V_K)$$

$$I_{s2} = g_{s2} s_2 (V - V_K)$$

Gating and other functions:

$$m_\infty = \frac{1}{1 + e^{\frac{V_m - V}{s_m}}}$$

$$n_\infty = \frac{1}{1 + e^{\frac{V_n - V}{s_n}}}$$

$$\tau_n = \frac{\bar{\tau}_n}{1 + e^{\frac{V - V_n}{s_n}}}$$

$$s_{1\infty} = \frac{1}{1 + e^{\frac{V_{s1} - V}{s_{s1}}}}$$

$$s_{2\infty} = \frac{1}{1 + e^{\frac{V_{s2} - V}{s_{s2}}}}$$

Paramater	Values	Parameter	Values
V_l (mV)	-40	g_{s1}(pS)	32
V_{Ca} (mV)	100	g_{s2}(pS)	3
V_K (mV)	-80	$C_m(\mu\text{F/cm}^2)$	4524
λ	1.1	$\bar{\tau}_n$ (ms)	9.09
g_{Ca} (pS)	280	V_m (mV)	-22
g_K (pS)	1300	V_n (mV)	-9
g_l (pS)	25	s_m	7.5
V_{s1}(mV)	-40	s_n	10
τ_{s1}(ms)	1000	s_{s1}	0.5
V_{s2}(mV)	-42	s_{s2}	0.4
τ_{s2}(ms)	1.2×10^5		

2.1.4 Dual Oscillator Model (2007)

In 2004, Bertram and Sherman [8] proposed a model using the phantom bursting mechanism with 3 slow processes ($[Ca^{+2}]_i$, $[Ca^{+2}]_{ER}$, and ATP/ADP). In a later model, called the Dual Oscillator Model [9] (DOM), they combined this model with a model of glycolysis [10] and a model for mitochondrial metabolism [11,12]. A schematic of the DOM is shown in figure 2.3.

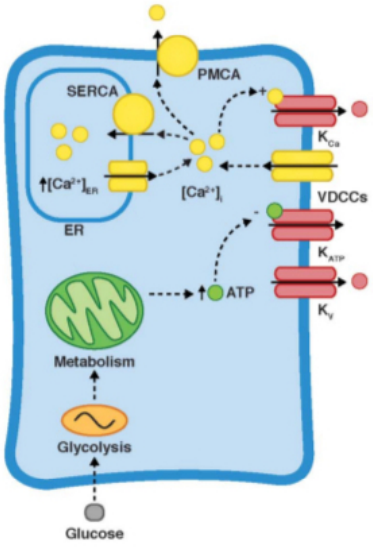

The interactions between the glycolytic, metabolic and electrical components drive different electrical behaviours depending on the regime of the glycolytic and electrical components. ATP production is controlled by the rate at which glucose is metabolized. Changes in ATP levels mediates the conductance of K_{ATP} channels, depolarization and Ca^{+2} influx. All three compartments are affected by changes in $[Ca^{+2}]_i$.

Figure 2.3: *Schematic of the Dual Oscillator Model [14]*

The Model Equations

The differential equations:

$$C_m \frac{dV}{dt} = -\left(I_K + I_{Ca} + I_{K(Ca)} + I_{K(ATP)}\right)$$

$$\frac{dn}{dt} = \frac{n_\infty(V) - n}{\tau_n}$$

$$\frac{dCa}{dt} = f_{cyt}(J_{mem} + J_{er})$$

$$\frac{dCa_{er}}{dt} = -f_{er}\left(\frac{V_{cyt}}{V_{er}}\right)J_{er}$$

$$\frac{dG6P}{dt} = \lambda(R_{GK} - R_{PFK})$$

$$\frac{dFBP}{dt} = \lambda\left(R_{PFK} - \tfrac{1}{2}R_{GPDH}\right)$$

$$\frac{dATP}{dt} = \frac{ATP - ADPe^{[(r+\gamma\}(1-ca/r_1)]}}{\tau_a}$$

The ionic currents:

$$I_K = \bar{g}_K n(V - V_K)$$

$$I_{Ca} = \bar{g}_{Ca} m_\infty(V)(V - V_{Ca})$$

$$I_{K(Ca)} = g_{K(Ca)}(V - V_K)$$

$$I_{K(ATP)} = g_{K(ATP)}(V - V_K)$$

Cytosolic and ER calcium dynamics:

$$J_{mem} = \alpha I_{Ca} + k_{PMCA} Ca$$

$$J_{er} = J_{leak} - J_{SERCA}$$

$$J_{leak} = p_{leak}(Ca_{er} - Ca)$$

$$J_{SERCA} = K_{SERCA} Ca$$

Other functions:

$$g_{K(Ca)} = \bar{g}_{K(Ca)} \frac{Ca^2}{K_D^2 + Ca^2}$$

$$g_{K(ATP)} = \bar{g}_{K(ATP)} o_\infty(ADP, ATP)$$

$$n_\infty(V) = \frac{1}{1+e^{-(16+V)/5}}$$

$$m_\infty(V) = \frac{1}{1+e^{-(20+V)/12}}$$

$$o_\infty(ADP,ATP) = \frac{0.08\left(1+\frac{2MgADP^-}{17\mu M}\right)+0.89\left(\frac{MgADP^-}{17\mu M}\right)}{\left(1+\frac{MgADP^-}{17\mu M}\right)^2\left(1+\frac{ADP^{3-}}{26\mu M}+\frac{ATP^{4-}}{1\mu M}\right)}$$

Nucleotide concentrations:

$$A_{tot} = AMP + ADP + ATP$$

$$AMP = \frac{ADP^2}{ATP}$$

$$MgADP^- = 0.165 ADP$$

$$ADP^{3-} = 0.135 ADP$$

$$ATP^{4-} = 0.05 ATP$$

Glycolysis:

$$w_{ikjl} = \frac{1}{f_{13}^{ik} f_{23}^{jk} f_{41}^{il} f_{42}^{jl} f_{43}^{kl}} \left(\frac{AMP}{K_1}\right)^i \left(\frac{FBP}{K_2}\right)^j \left(\frac{F6P}{K_3}\right)^k \left(\frac{ATP^2}{K_4}\right)^l$$

$$R_{PFK} = V_{max} \frac{(1-\lambda) w_{1110} + \lambda \sum_{ijl} w_{ijl1}}{\sum_{ijkl} w_{ijkl}}$$

$$F6P = 0.3 G6P$$

$$R_{GPDH} = 0.2\sqrt{FBP}$$

Parameter	Value	Parameter	Value	Parameter	Value
λ	0.06	$K_1(\mu\text{M})$	30	K_2 (μM)	1
K_3 (μM)	5×10^4	K_4 (μM)	220	f_{23}	0.2
f_{41}	20	f_{42}	20	f_{43}	20
C(fF)	5300	τ_n(ms)	20	$\bar{g}_K$(pS)	2700
$\bar{g}_{Ca}$(pS)	1000	$\bar{g}_{KATP}$(pS)	2.5×10^4	V_K(mV)	-75
V_{Ca}(mV)	25	$K_D(\mu\text{M})$	0.5	α (μM/ms)	4.5×10^{-6}
$k_{pmca}(\text{ms}^{-1})$	0.1	$p_{leak}(\text{ms}^{-1})$	2×10^{-4}	$k_{SERCA}(\text{ms}^{-1})$	0.4
f_{er}	0.01	f_c	0.01	$\frac{V_{Cyt}}{V_{er}}$	31
V_{max}(mV)	2	$A_{tot}(\mu\text{M})$	3000	ν_γ	2.2
$k_\gamma(\mu\text{M/s})$	10	$R_{GK}(s^{-1})$	0.2	$K_{dd}(\mu\text{M})$	17
$K_{td}(\mu\text{M})$	26	$K_{tt}(\mu\text{M})$	1	τ_a(ms)	3×10^5
r	1	$r_1(\mu\text{M})$	0.35	$\bar{g}_{K(Ca)}$(pS)	600

2.2 Methods

2.2.1 Coupled Map Lattices to Model Islets

Coupled Map Lattices is a method to model the collective dynamics of a system with interacting parts. I have modelled the pancreatic islet as a 1D ring of cells (with periodic boundary conditions, *Fig. 2.4)*. Each cell is coupled to its nearest neighbour. Biologically, coupling is achieved through the presence of gap junctions in the membranes of adjoining cells which allows small molecules and ions to pass through. Hence, neighbouring cells can sense voltage differences through the gap junctions. In the 1D ring, each lattice site (or cell) is described by the DOM system of equations.

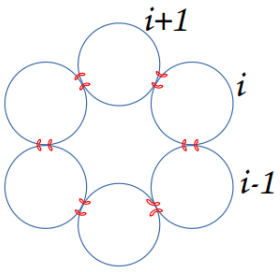

Figure 2.4: *1D ring of coupled cells*

The effect of coupling is modelled by changing the form of the voltage differential equation. Equation (1.4) is modified such that the voltage variation of the i^{th} cell can be written as:

$$C_m \frac{dV_i}{dt} = -\sum I_{ionic} - \mathbf{g_c}(\mathbf{V_{i-1}} - \mathbf{V_i}) - \mathbf{g_c}(\mathbf{V_i} - \mathbf{V_{i+1}})$$

where, g_c is the gap junction coupling strength between two adjacent cells and V_{i+1} and V_{i-1} are the voltages of the two nearest neighbours of the i^{th} beta cell.

2.2.2 Synchronization Order Parameter, R

The Synchronization Order Parameter [13], R, is a measure of spatio-temporal synchronicity in a population of coupled oscillators (here beta cells). The value of R indicates the level of synchronization by comparing the average of the local signal (here membrane voltage of a beta cell) to the global behaviour. R is explicitly defined as follows:

$$R = \frac{\langle M^2 \rangle - \langle M \rangle^2}{\left[\langle z_i^2 \rangle - \langle z_i \rangle^2 \right]}$$

where [] denotes spatial averaging and $\langle\rangle$ denotes temporal averaging. M is the spatial average of z_i (voltage values in the case of coupled beta cells) over N cells at every time point. R takes up values between 0 and 1. If all the beta cells are completely synchronized with respect to their electrical activity, then the average of the local signal will be the same as the global behaviour. Hence, R ~ 1. If the beta cells are unsynchronized, the individual states will be different and hence R ~ 0.

All simulations were programmed on MATLAB R2012b using the ode15s ode solver, and run on a Workstation with an Intel® Xeon(R) CPU E5-1620 0 @ 3.60GHz × 8 processor. The operating system used was Ubuntu v14.04 LTS (64-bit). It took approximately 5 days to run a 10^7ms simulation of coupled beta cells.

Chapter 3

Results

The results are organized in the following manner: First, the simulation results of the single beta cell bursting dynamics for the four models mentioned in the Models section of Chapter 2 are shown, and their drawbacks mentioned. Second, since the Dual Oscillator Model (DOM) is the only model capable of reproducing most experimental results, simulation results of two cells (each described by the DOM) coupled through gap junctions are shown. Finally, simulation results for a ring-like, one-dimensional CML model of an islet with multiple beta cells, each described by the DOM, coupled to their nearest two neighbours are shown. For both the two and multiple cell models, simulations of a 1D ring of both homogeneous and heterogeneous beta cells (in terms of bursting dynamics) is shown.

3.1 Single Cell Results

3.1.1 Chay-Keizer Model Predictions

The burst pattern and calcium oscillations simulated using the CK model equations (see section 2.1.1) are shown in figure 3.1(a), for the following initial conditions: v0 = -54.774; n0 = 0.00044035; mca0 = 0.027532; hca0 = 0.086321; ca0 = 0.10749 (All the values for each of the parameters used are mentioned in the previous chapter). The experimentally observed time curves are shown in figure 3.1(b). It is clear that the CK model predicts a slower and different form of the calcium dynamics than observed experimentally.

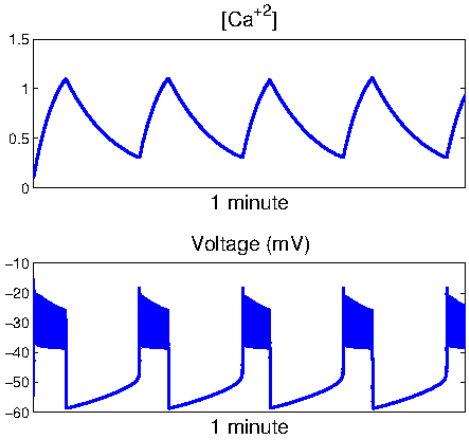

(a) Top: CK predicts the $[Ca^{+2}]_i$ time curve to be square wave. Bottom: CK predicts the voltage time curve to be square wave with bursting. *(KCa = 0.04;* g_{KCa} *= 0.09)*

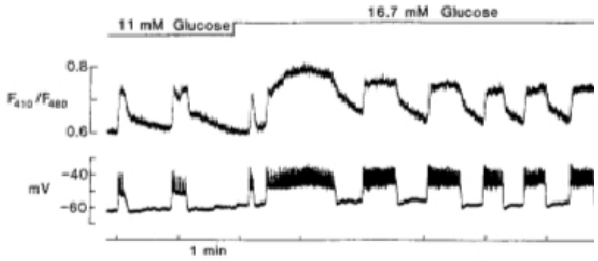

(b) Top: Experimentally observed $[Ca^{+2}]_i$ time curve. Bottom: Experimentally observed voltage time curve [1]

Figure 3.1: ***(a)*** *CK model predicted time curves* ***(b)*** *Experimentally observed time curves.*

Moreover, it was experimentally found that blocking K_{Ca} channels with charybdotoxin produced no significant effect on the electrical activity [3]. However, modelling the blocking of K_{Ca} channels leads to a disruption in the burst pattern *(Fig. 1.2 (a)).*

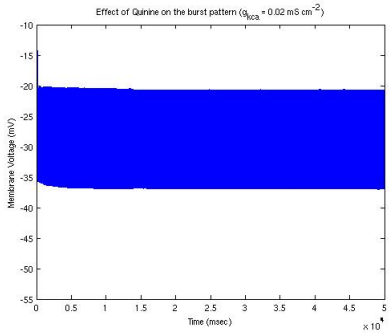

(a) CK model predicts a loss in burst pattern on blockage of K_{Ca} channels by charybdotoxin/quinine. *(KCa = 0.001;* g_{KCa} *= 0.09)*

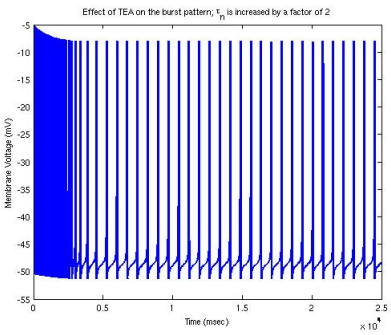

(b) CK model predicts an increase in the voltage dynamics when K_V channels are blocked by TEA. *(KCa = 0.04;* g_{KCa} *= 0.02)*

Figure 3.2: ***(a)*** *CK model predicted burst pattern when* K_{Ca} *channels are blocked* ***(b)*** *CK model predicted burst pattern when* K_V *channels are blocked by TEA*

The hypothesis proposed by the CK model was discarded when $[Ca^{+2}]_i$ was measured (experimentally) [1,2] in beta cells, revealing different and more rapid dynamics than predicted by the CK model.

3.1.2 Smolen-Keizer Model Predictions

The burst pattern and calcium oscillations simulated using the SK model equations (see section 2.1.2) are shown in figure 3.3, for the following initial conditions: v0=-53; n0=0.002; ca0=0.15; d0=0.42; pc0=0.9; pot0=0.02; ii0=0.98; jj0=0.47 (All the values for each of the parameters used are mentioned in the previous chapter).

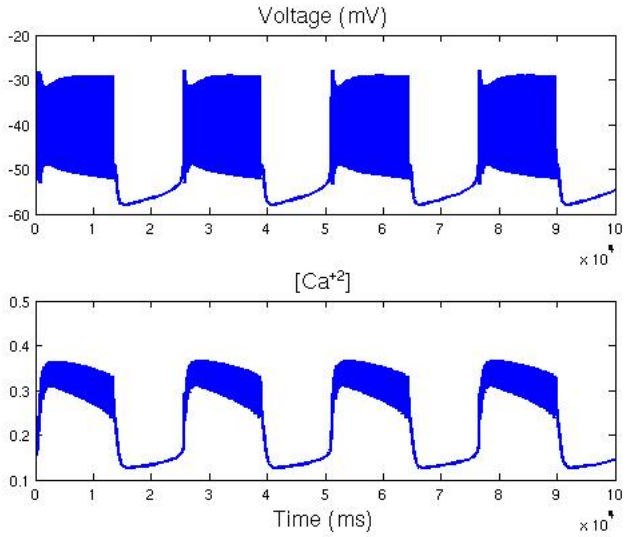

Figure 3.3: *The SK model is able to reproduce the fast dynamics of* $[Ca^{+2}]_i$ *oscillations*

Dufer *et. al.* [4] report that electrical activity in beta cells lacking functional K_{ATP} channels persists. All the models (including the SK model) that are based on the oscillations of the ATP/ADP ratio to produce bursting electrical activity by regulating the conductance of the K_{ATP} channels are unable to reproduce this observation. However, the SK model is able to reproduce the fast dynamics of $[Ca^{+2}]_i$ oscillations, and in fact, includes an improved model of the Ca^{+2} currents *(Fig. 1.2 (b))*.

3.1.3 Phantom Burster Model Predictions

The possible burst patterns simulated using the PB model equations (see section 2.1.3) are shown in figure 3.4(a), for the following initial conditions: v0 = -43.0; n0 = 0.03; s10 = 0.1; s20 = 0.434 (All the values for each of the parameters used are mentioned in the previous chapter). The experimentally observed burst patterns are shown in figure 3.4(b). In the model the value for 'gs1' is changed to see bursting with different time periods. gs1 = 3 for slow bursting; gs1 = 4 for intermediate, 'phantom bursting'; gs1 = 20 for fast bursting.

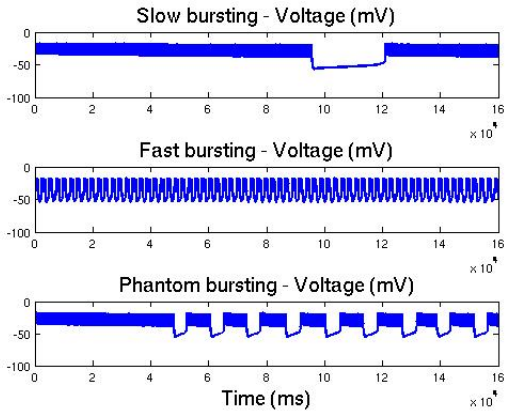

(a) The PB model can reproduce slow (top, *gs1=3*), fast (middle, *gs1=20*) and phantom (bottom, *gs1=4*) voltage dynamics.

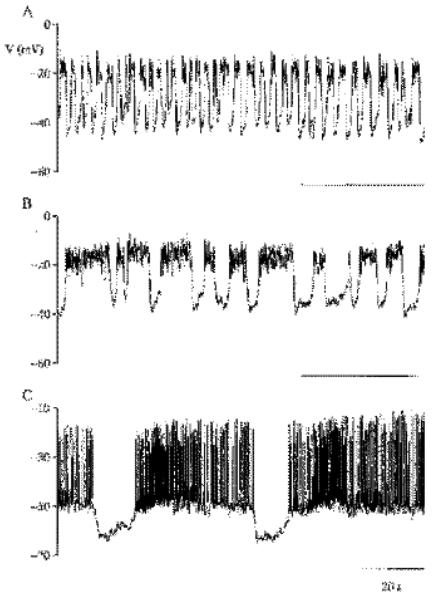

(b) Experimentally observed burst patterns on fast (A), medium (B), and slow (C) time scales [9]

Figure 3.4: ***(a)*** *PB model predicted possible voltage dynamics* ***(b)*** *Experimentally observed voltage dynamics*

Single cell electrophysiological studies [5,6] have established that single cells can burst as well as spike repetitively, but this bursting is typically much faster than that in islets. Sometimes bursts much slower than those in islets (period 1–6 min) [7,8] are seen. Bursting with a period comparable to that in islets is seen, but only rarely. The Phantom Burster model is capable of reproducing bursting of all these periodicities. The phantom bursting is significant in light of the fact that no slow process with a medium-scale time constant has been identified in beta cells.

3.1.4 Dual Oscillator Model Predictions

The burst pattern and calcium oscillations simulated using the DOM equations (see section 2.1.4) are shown in figure 3.5(a), for the following initial conditions: V0 = -60; n0 = 0; Ca0 = 0.1; CaER0 = 185; ADP0 = 780; G6P0 = 200; FBP0 = 40 (All the values for each of the parameters used are mentioned in the previous chapter).

The different types of bursting are reproduced by changing the values of R_{GK} (Rate of the enzyme *Glucokinase*), g_{KATP} (conductance of the ATP dependent potassium channel) and g_{KCa} (conductance of the calcium dependent potassium channel) values.

For Slow bursting: R_{GK} = 0.2; gKATP = 27000; gKCa = 100;

For Fast bursting: R_{GK}= 0.4; gKATP = 25000; gKCa = 600;

For Subthreshold bursting: R_{GK}= 0.2; gKATP = 30000; gKCa = 100;

For Compound bursting: R_{GK} = 0.2; gKATPbar = 25000; gKCabar = 600;

For Accordian bursting: R_{GK}= 0.2; gKATP = 23000; gKCa = 600;

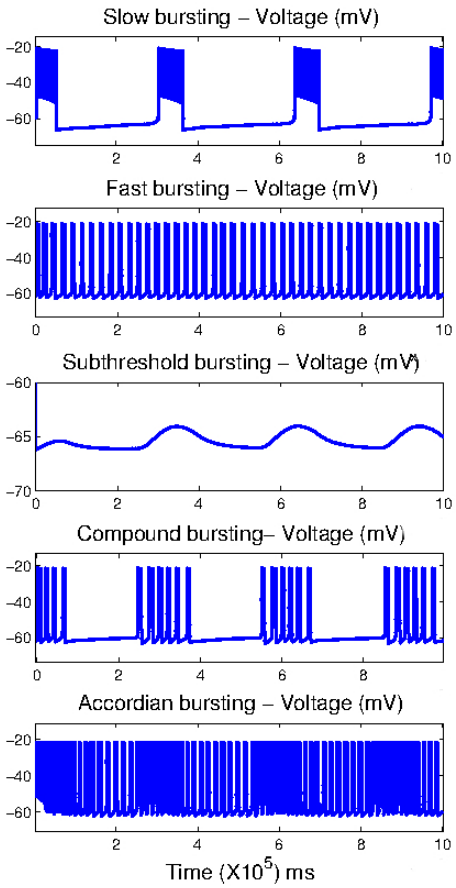

(a) DOM reproduces the full repertoire of bursting 'types' for different R_{GK}, g_{KATP} and g_{KCa} values.

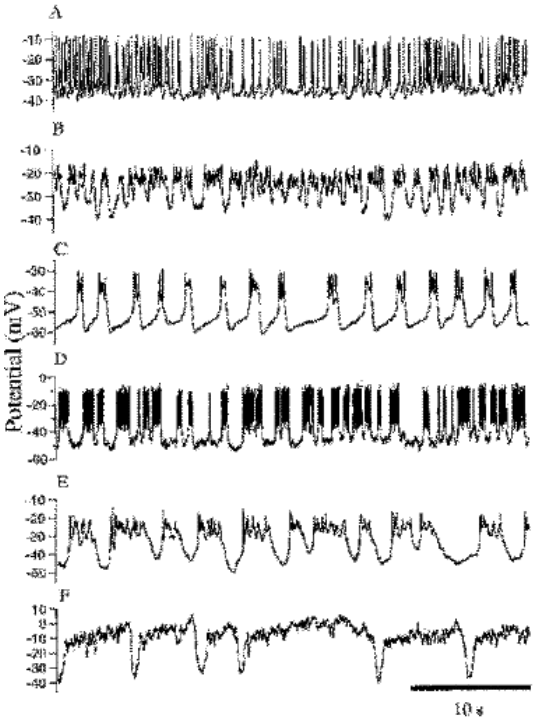

(b) Experimental recordings of different burst patterns in single mouse beta cells [5]

Figure 3.5: ***(a)*** *DOM predicted repertoire of bursting* ***(b)*** *Experimental observations*

The DOM reproduces the full range of periods observed in electrical bursting activity (including the compound and mixed oscillations), seen experimentally [5]. Most of the predications of the DOM have acquired experimental verification. For example; the DOM predicts oscillations in the glycolytic pathway, which has been seen in direct experimentation [10]. The DOM is the only model capable of reproducing the following experimental observation: sub-threshold metabolic oscillations in the absence of $[Ca^{+2}]_i$ oscillations [11] *(Fig. 3.4 (a)).*

A point to note is that, like every other model, the DOM cannot explain the observation made by Dufer *et. al.* [4], that the electrical activity in beta cells lacking functional K_{ATP} channels persists.

The DOM is a really elegant model because of the incorporation of glycolytic, metabolic and electrical components of the beta cell. There is a clear connection between the electrical activity of the membrane and the global function of the beta cell in the secretion of insulin. Since almost all the predictions of the DOM have experimental support, the Dual Oscillator Model was used to simulate a collection of coupled beta cells - the *Islet of Langerhans.*

3.2 Coupled Cell Results

Simulation results of beta cells (described by the DOM) coupled via gap junctions are shown. All the constituent cells in the coupled system can have the same dynamics (Homogeneous), or can be a mix of more than one type of bursting dynamics (Heterogeneous).

3.2.1 Homogeneous Cells

First, how coupling two cells (via gap junctions) may change the individual bursting behaviour of each cell is shown. Second, the emergent, collective behaviour of an islet is shown by coupling 30 beta cells in a 1D ring with periodic boundary conditions.

3.2.1.1 Two Cells

The voltage differential equation for two coupled cells is:

$$\text{For Cell 1: } C_m \frac{dV_1}{dt} = -I_{ionic} - g_c(V_1 - V_2)$$

$$\text{For Cell 2: } C_m \frac{dV_2}{dt} = -I_{ionic} - g_c(V_2 - V_1)$$

The burst frequency and length of burst stabilizes for coupling strengths > 100pS when two identical cells are coupled.

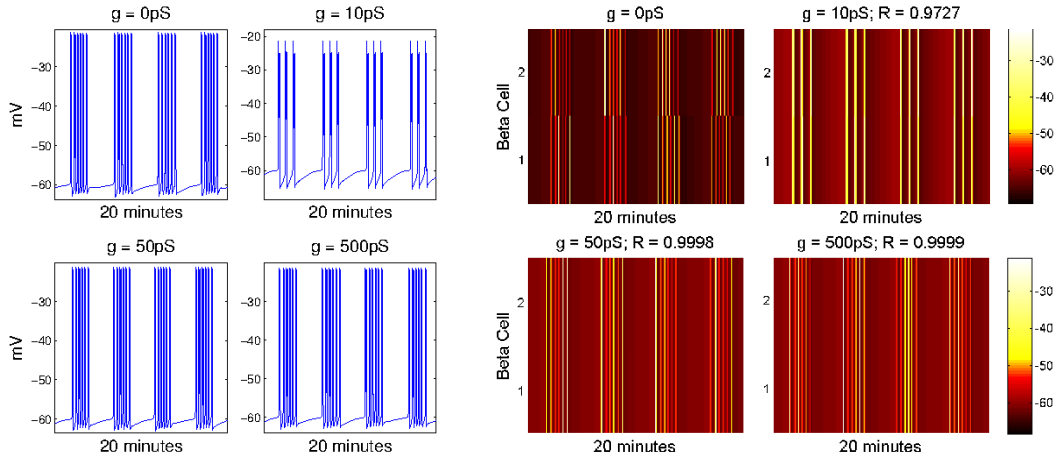

(a) Voltage time curves (for different g_cs)

(b) Corresponding space-time plots with the synchronisation order parameter, R, given for coupled cells.

Figure 3.6: ***(a)*** *Voltage time curves (for different g_cs) for two coupled compound cells* ***(b)*** *Corresponding space-time plots*

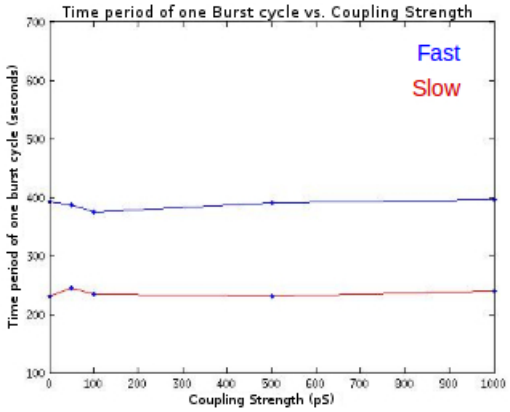

(a) Time period of one cycle (Burst followed by silent phase) versus coupling strength, g_c.

As can be seen in figure 3.7(a), the time period of one cycle (burst followed by the silent phase) stabilizes when the coupling strength increases beyond ~100pS. In addition, the percentage of the time period spent bursting also stabilizes. This is true when any two identical (fast, slow, accordian or compound) cells are coupled together.

Figure 3.7: *Time period of one cycle stabilizes for g_c> 100pS*

3.2.1.2 Thirty Cells

On coupling thirty homogeneous cells the burst pattern, time period and burst percentage is lost when g_c is increased. For intermediate g_c values (~100pS to 500pS) the burst pattern is completely lost and replaced by high frequency oscillations.

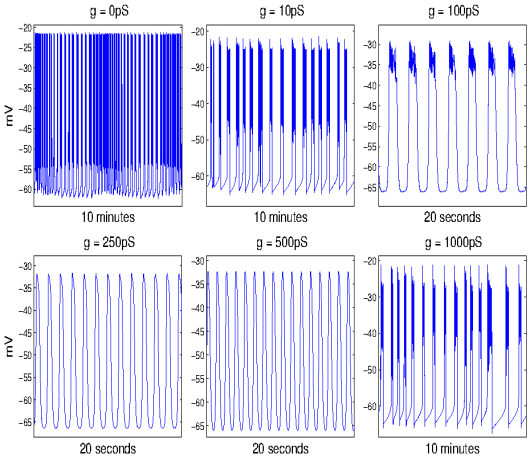

(a) Voltage time curves (for different g_cs) for 30 coupled accordian cells.

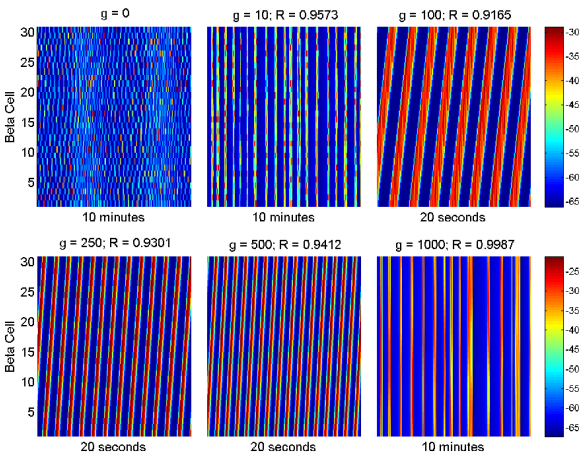

(b) Corresponding space-time plots with R given for coupled cells.

Figure 3.8: *Voltage time curves and space-time plots for 30 coupled accordian cells*

The specific pattern of the space-time plots for intermediate $g_c$values (~100pS, 250pS and 500pS) indicates that the high frequency oscillations of individual beta cells is actually a wave travelling through the ring of beta cell. The wave travels through the lattice with uniform velocity.

The table in figure 3.9 shows how the time period of one cycle and the percentage of the time period spent on bursting changes as $g_c$is increased (for each of the different

cell types). For each homogeneous 1D ring (and each g_c value) multiple simulations of length between 10^7 and 10^8 ms were run and the time period values were calculated after a suitable period of transient time was allowed to pass.

	g = 0pS	g = 10pS	g = 10^2pS	g = 250pS	g = 500pS	g = 10^3pS
Accordian	~4.6 mins	~4mins	2 secs (~75%)	2 secs (Osci.)	1.5 secs (Osci.)	Variable (~25%)
Compound	5mins (~60%)	5 mins (~60%)	2 secs (~90%)	2 secs (Osci.)	2 secs (Osci.)	5.2 mins (~65%)
Fast	23 secs (~67%)	54 secs (~80%)	3 secs (~70%)	1.5 secs (Osci.)	2 secs. (Osci.)	Variable (~18%)
Slow	40 secs (~70%)	Variable (~19%)	3 secs (~50%)	2 secs (Osci.)	2 secs (Osci.)	57 secs (~83%)

Figure 3.9: *Time period of one cycle and % of time period spent on bursting changes for increasing g_c.*

The cells synchronize their burst and silent phases for low and high coupling strengths. However, for low coupling strengths the bursting time course of neighbouring cells is 180° out of phase. As coupling strength increases, bursting becomes more in phase. For very high coupling strengths bursting is completely in phase.

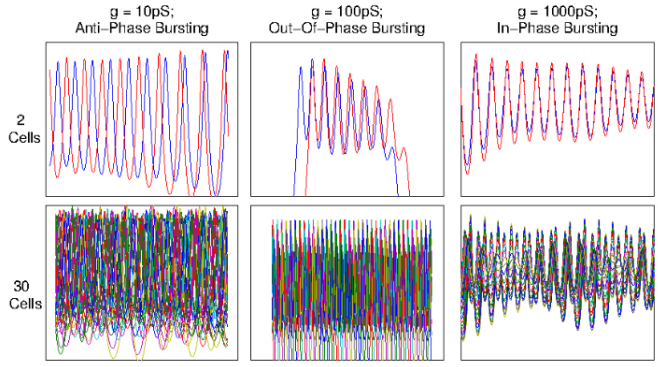

In figure 3.10, the top panel shows the superimposed time curves of two neighbouring cells (for different g_cs). The bottom panel shows the superimposed time curves of all 30 cells in the 1D ring. As can be seen, the variation between the time curves is less for a very high g_c value.

Figure 3.10: *Synchronization of bursts goes from 180° anti-phase (low g_c), to out-of-phase, to completely in-phase (high g_c).*

3.2.2 Heterogeneous Cells

First, how coupling two different cells may lead to emergent bursting behaviour of a different type is shown. Second, the emergent, collective behaviour of a heterogeneous islet is shown by coupling 32 beta cells in a 1D ring with periodic boundary conditions.

3.2.2.1 Two Cells

Emergent accordian type behaviour is seen on coupling a slow and a compound cell or a fast and a compound cell *(Fig. 3.11)*.

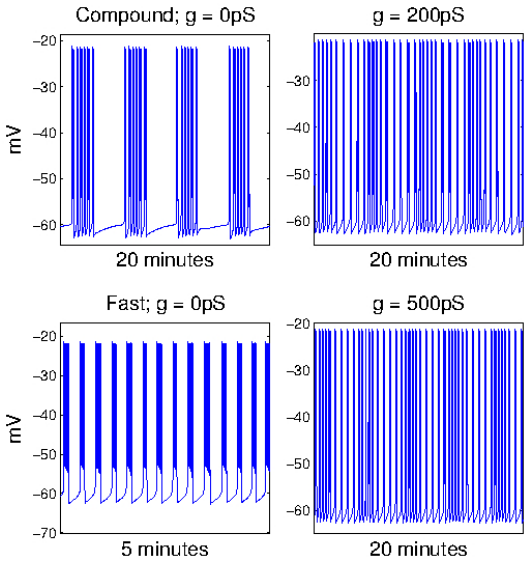

(a) Coupled Fast and Compound: Voltage time curves (for different g_cs)

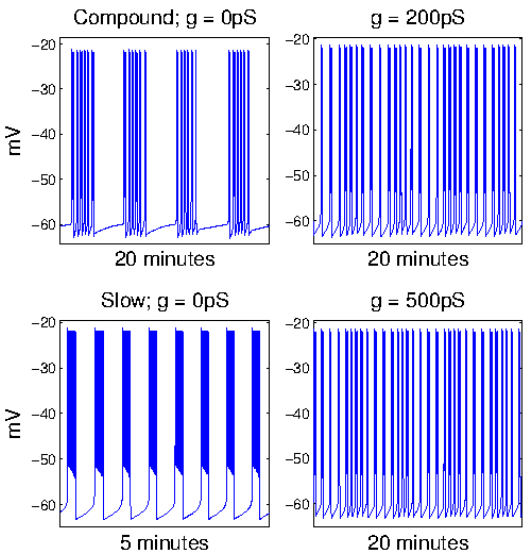

(b) Coupled Slow and Compound: Voltage time curves (for different g_cs)

Figure 3.11: *Emergent accordian behaviour is seen on coupling a fast/slow cell with a compound cell.*

Coupling any other cell types leads to behaviour intermediate to that of the original two cell types.

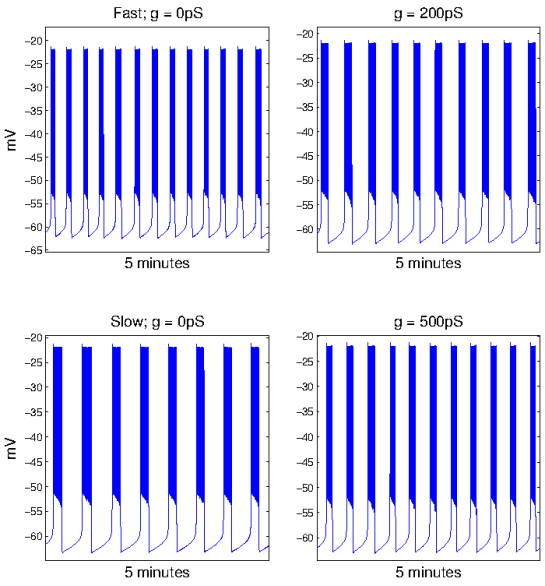

(a) Voltage time curves for different g_cs for a fast-slow coupled pair of cells.

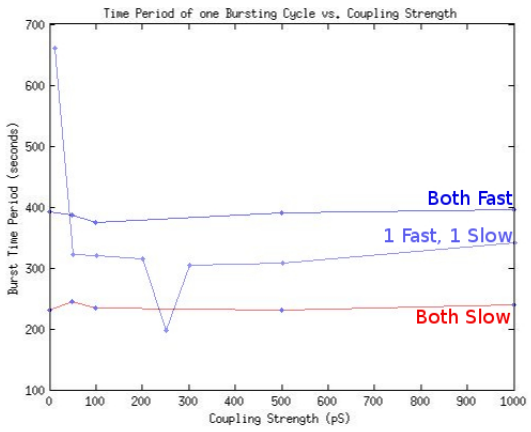

(b) The time period of one cycle for a fast-slow coupled pair is intermediate to that of the only fast/only slow situation.

Figure 3.12: *Intermediate behaviour of a fast-slow coupled pair of cells.*

3.2.2.2 Thirty-Two Cells

For large number of cells, coupling of compound and fast/slow types does not lead to emergent accordian type bursting behaviour – instead, the behaviour of such a ring of cells is similar to that of a homogeneous ring of accordian cells *(Fig. 3.13).*

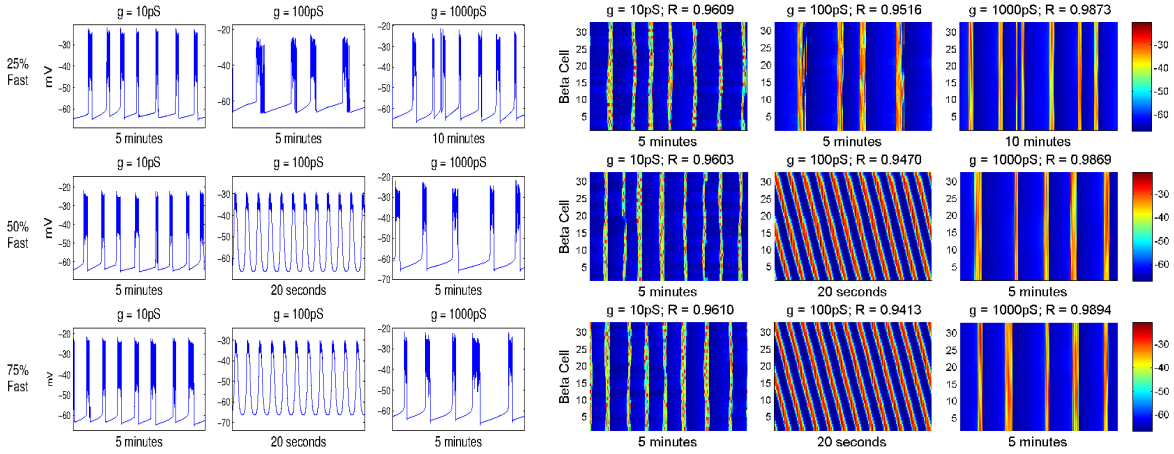

(a) Voltage time curves for 32 coupled cells with varying percentages of compound and fast cells.

(b) Corresponding space-time plots with R given for coupled cells.

Figure 3.13: *Coupling large number of compound and fast/slow cells doesn't lead to emergent accordian behaviour.*

As the percentage of fast cells increases to 100%, the burst time percentage approaches that of the burst percentage of a homogeneous ring of Fast cells.

The table in figure 3.14 shows how the percentage of the time period spent on bursting changes as g_c is increased and the percentage of fast cells in a mixture of fast and compound cells is changed. For each heterogeneous 1D ring (and each g_c value) multiple simulations of length between $5X10^6$ and 10^8 ms were run and the values were calculated after a suitable period of transient time was allowed to pass.

	g=0pS	g=10pS	g=10²pS	g=10³pS
0% Fast	~40%	~40%	~50%	~36%
25% Fast	-	~17%	~30%	~19%
50% Fast	-	~19%	~25%	~15.4%
75% Fast	-	~20%	~27.5%	~14.8%
100% Fast	~33.3%	~20%	~33.3%	~15%

Figure 3.14: *Burst percentage changes with changing coupling strength and percentage of fast cells in a mixture of fast and compound cells.*

Chapter 4

Concluding Remarks

When single units interact, often what is seen is that the behaviour of such a collection of interacting units is different from the behaviour of each individual unit - emergent behaviour. Such is the case with pancreatic beta cells. The dynamics of a single beta cell is extremely different from that of a cluster of coupled cells. The presence of gap junctions between neighbouring beta cells in an islet forces each individual cell to 'talk' to its neighbouring cells. As a consequence, all the cells in the islet behave in a synchronized manner. This synchronization is absolutely essential in the proper functioning of the pancreas; to properly respond to elevated blood glucose levels by secreting insulin in a pulsatile fashion.

Synchronization of the electrical (hence insulin secreting) activity on coupling beta cells means that the body is more tolerant to the presence of a greater variety of beta cells in different 'states' (initial conditions and parameter values). Through this study I have tried to understand how emergent, synchronized behaviour is achieved on coupling cells.

Conclusions

1. When two homogeneous cells are coupled together (both accordian or compound or fast or slow), the time period of one cycle (burst followed by silent phase) and percentage of time spent bursting stabilizes for g_c values greater than ~100pS. No emergent behaviour is seen.

2. When two cells, one compound and the other fast or slow, are coupled together emergent accordian type behaviour is seen. This emergent accordian pattern has the same time period (~300 seconds) as the 'original' accordian type cell. However, the emergent accordian pattern is less dense than the original one.

3. When multiple homogeneous cells are coupled together the original burst pattern of a single cell is lost. For low coupling strengths (g_c<~200pS) the burst

pattern becomes irregular. For intermediate coupling strengths (~250pS < g_c< ~500pS) bursting behaviour is lost and replaced by high frequency (1.5-2 seconds) oscillations. For high coupling strengths (g_c> 1000pS) the irregular bursting pattern is recovered.

4. On observing the space-time plots (~250pS < g_c< ~500pS) of multiple homogeneous coupled cells, it appears that the high frequency oscillations are actually travelling waves that move around the ring with uniform velocity.

5. Synchronization of volatge time curves during bursts goes from 180˚ anti-phase (low g_c), to out-of-phase (intermediate g_c), to completely in-phase (high g_c). Hence, R~1 is seen only when g_c is very high (>1000pS).

6. When multiple cells (of compound and fast or slow) are coupled together, the emergent accordian pattern seen when a pair of cells is coupled, is lost. Irregular bursting and high frequency oscillations are seen (just like the homogeneous case).

7. In a mixture of fast and compound cells, as the percentage of fast cells increases towards 100%, the percentage of time spent bursting by the group of cells tends to that of the case where all the coupled cells are of only fast type.

Future Directions

1. The effect of heterogeneous coupling has not been studied. It would be interesting to see if and how the results would change by incorporating different coupling strengths among pairs of cells.

2. The 1D ring with periodic boundary conditions can be modified to a 1D ring with fixed boundary conditions.

3. The 1D ring can be extended to 2D or even 3D lattices.

Given that beta cell dysfunction is implicated in Type 2 Diabetes, most likely, models of human beta cells will evolve and develop rapidly. Hopefully, these models will be biologically sufficiently complicated that they will be able to contribute to the design and prediction of new therapies and drugs; while being mathematically sufficiently simple enough that mathematical biologists may analyze and simulate them.

Chapter 5

References

Chapter 1

1. Matthews DR, Lang DA, Burnett MA, Turner RC. Control of pulsatile insulin secretion in man. Diabetologia 1983; 24:231-7; PMID:6345247; http://dx. doi.org/10.1007/BF00282705

2. Hellman B. Pulsatility of insulin release – a clinically important phenomenon. Ups J Med Sci 2009; 114:193-205; PMID:19961265; http://dx.doi.org/ 10.3109/03009730903366075

3. Lang DA, Matthews DR, Burnett M, Turner RC. Brief, irregular oscillations of basal plasma insulin and glucose concentrations in diabetic man. Diabetes 1981; 30:435-9; PMID:7014311; http://dx.doi. org/10.2337/diab.30.5.435

4. http://mrrittner.weebly.com/uploads/1/3/7/1/13714989/108203_orig.jpg

5. https://upload.wikimedia.org/wikipedia/commons/thumb/3/33/ MembraneCircuit.jpg/500px-MembraneCircuit.jpg

6. Serre-Beinier, V *et. al.* Cx36 Preferentially Connects Cells Within Pancreatic Islets. Diabetes, Vol. 49, (2000). 10.2337/diabetes.49.5.727

7. Serre-Beinier, V *et. al.* Cx36 preferentially connects cells within pancreatic islets. Diabetes 49:727–734, 2000 8.

8. Theis M *et. al.* Replacement by a lacZ reporter gene assigns mouse connexin36, 45 and 43 to distinct cell types in pancreatic islets. Exp Cell Res 294:18 –29, 2004

9. MacDonald PE, Rorsman P (2006) Oscillations, intercellular coupling, and insulin secretion in pancreatic Beta cells. PLoS Biol (4)2: e49.

10. Hodgkin, A. L.; Huxley, A. F. (1952). A quantitative description of membrane current and its application to conduction and excitation in nerve. The Journal of Physiology 117 (4): 500–544. doi:10.1113/jphysiol.1952.sp004764. PMC 1392413. PMID 12991237.

11. T.A. Kinard, G. de Vries, A. Sherman, L.S. Satin. Modulation of the bursting properties of single mouse pancreatic beta cells by artificial conductances. Biophys. J., 76 (1999), pp. 1423–1435

Chapter 2

1. Chay TR, Keizer J. Minimal model for membrane oscillations in the pancreatic b-cell. Biophys J 1983; 42:181-9; PMID:6305437; http://dx.doi.org/ 10.1016/S0006-3495(83)84384-7

2. Hodgkin, A. L.; Huxley, A. F. (1952). A quantitative description of membrane current and its application to conduction and excitation in nerve. The Journal of Physiology 117 (4): 500–544. doi:10.1113/jphysiol.1952.sp004764. PMC 1392413. PMID 12991237.

3. Atwater I, Rosario L, Rojas E. Properties of the Ca-activated K^+ channel in pancreatic b-cells. Cell Calcium 1983; 4:451-61; PMID:6323007; http://dx. doi.org/10.1016/0143-4160(83)90021-0

4. Cook D. Intracellular ATP directly blocks K^+channels in pancreatic B-cells. Nature 1984; 311:271-3; PMID:6090930; http://dx.doi.org/10.1038/ 311271a0

5. Ashcroft FM, Harrison DE, Ashcroft SJH. Glucose induces closure of single potassium channels in isolated rat pancreatic b-cells. Nature 1984; 312:446- 8; PMID:6095103; http://dx.doi.org/10.1038/ 312446a0

6. Smolen P, Keizer J. Slow voltage inactivation of Ca^{+2} currents and bursting mechanisms for the mouse pancreatic beta-cell. J Membrane Biol 1992; 127:9-19; http://dx.doi.org/10.1007/BF00232754

7. Bertram R, Previte J, Sherman A, Kinard TA, Satin LS. The phantom burster model for pancreatic b-cells. Biophys J 2000; 79:2880-92; PMID: 11106596; http://dx.doi.org/10.1016/S0006-3495(00) 76525-8

8. Bertram R, Sherman A. A calcium-based phantom bursting model for pancreatic islets. B Math Biol 2004; 66:1313-44; http://dx.doi.org/10.1016/j. bulm.2003.12.005

9. Bertram R, Sherman A, Satin LS. Metabolic and electrical oscillations: partners in controlling pulsatile insulin secretion. Am J Physiol Endocrinol Metab 2007;

293:E890-E900; PMID:17666486;
http://dx.doi.org/10.1152/ajpendo.00359.2007

10. Smolen P. A model for glycolytic oscillations based on skeletal muscle phosphofructokinase kinetics. J Theor Biol 1995; 174:137-48; PMID:7643610;
http://dx.doi.org/10.1006/jtbi.1995.0087

11. Magnus G, Keizer J. Model of b-cell mitochondrial calcium handling and electrical activity. II. Mitochondrial variables. Am J Physiol Cell Physiol 1998; 274:1158-73;

12. Magnus G, Keizer J. Model of b-cell mitochondrial calcium handling and electrical activity. I. Cytoplasmic variables. Am J Physiol Cell Physiol 1998; 274:1174-84.

13. J. Garcia-Ojalvo, Michael B. Elowitz, and Steven H. Strogatz. Modeling a synthetic multicellular clock: Repressilators coupled by quorum sensing. Proc. Natl. Acad. Sci. U.S.A. 2004; 101 , 10955

14. Chay TR. The effect of inactivation of calcium channels by intracellular Ca^{+2} ions in the bursting pancreatic beta cells. Cell Biophys 1987; 11(1): 77-90; PMID:2450671; http://dx.doi.org/10.1007/ BF02797114

15. Gilon P, Ravier MA, Jonas JC, Henquin JC. Control mechanisms of the oscillations of insulin secretion in vitro and in vivo. Diabetes 2002; 51 (Suppl 1):S144-51; PMID:11815474; http://dx. doi.org/10.2337/diabetes.51.2007.S144

16. Fridlyand LE, Tamarina N, Philipson LH. Bursting and calcium oscillations in pancreatic beta cells: specific pacemakers for specific mechanisms. Am J Physiol Endocrinol Metab 2010; 299:E517-32; PMID:20628025;
http://dx.doi.org/10.1152/ajpendo. 00177.2010

17. Smith PA, Ashcroft FM, Rorsman P. Simultaneous recordings of glucose dependent electrical activity and ATP-regulated K_{Ca} currents in isolated mouse pancreatic beta cells. FEBS Lett 1990; 261:187-90; PMID:2407553;
http://dx.doi.org/10.1016/0014- 5793(90)80667-8

18. Bertram R *et. al*. A role for calcium release-activated current (CRAC) in cholinergic modulation of electrical activity in pancreatic beta cells. Biophys J 1995; 2323-32; PMID:7647236; http://dx.doi.org/10.1016/S0006- 3495(95)80414-5

19. Chay TR. Electrical bursting and luminal calcium oscillation in excitable cell models. Biol Cybern 1996; 75:419-31; PMID:8983163;
http://dx.doi. org/10.1007/s004220050307

20. Kim A, Miller K, Jo J, Kilimnik G, Wojcik P, Hara M. Islet architecture: A comparative study. Islets 2009; 1:129-36; PMID:20606719; http://dx.doi. org/10.4161/isl.1.2.9480

21. Rorsman P, Braun M. Regulation of insulin secretion in human pancreatic islets. Annu Rev Physiol 2013; 75:155-79; PMID:22974438;

22. Braun M *et. al*. Voltage-gated ion channels in human pancreatic beta cells: electrophysiological characterization and role in insulin secretion. Diabetes 2008; 57:1618- 28; PMID:18390794; http://dx.doi.org/10.2337/ db07-0991

23. Braun M, Ramracheya R, Johnson PR, Rorsman P. Exocytotic properties of human pancreatic beta cells. Ann NY Acad Sci 2009; 1152:187-93; PMID:19161389; http://dx.doi.org/10.1111/ j.1749-6632.2008.03992.x

Chapter 3

1. Santos RM, Rosario LM, Nadal A, Garcia-Sancho J, Soria B, Valdeolmillos M. Widespread synchronous $[Ca^{+2}]_i$ oscillations due to bursting electrical activity in single pancreatic islets. Pflugers Arch 1991; 418:417-22; PMID:1876486; http://dx.doi.org/ 10.1007/BF00550880

2. Valdeolmillos M, Santos RM, Contreras D, Soria B, Rosario LM. Glucose-induced oscillations of intracellular Ca^{+2} concentration resembling bursting electrical activity in single mouse islets of Langerhans. FEBS Lett 1989; 259:19-23; PMID: 2689228; http://dx.doi.org/10.1016/0014-5793 (89)81484-X

3. Kukuljan M, Goncalves AA, Atwater I. Charybdotoxin-sensitive K_{Ca} channel is not involved in glucose-induced electrical activity in pancreatic beta cells. J Membrane Biol 1991; 119:187-95; http://dx.doi. org/10.1007/BF01871418

4. Dufer M, Haspel D, Krippeit-Drews P, Aguilar-Bryan L, Bryan J, Drews G. Oscillations of membrane potential and cytosolic Ca^{+2} concentration in SUR1 -/- beta cells. Diabetologia 2004; 47:488-98; PMID:14872319; http://dx.doi.org/10.1007/ s00125-004-1348-0

5. T.A. Kinard, G. de Vries, A. Sherman, L.S. Satin. Modulation of the bursting properties of single mouse pancreatic beta cells by artificial conductances. Biophys. J., 76 (1999), pp. 1423–1435

6. L.C. Falke, K.D. Gillis, D.M. Pressel, S. Misler. Perforated patch recording allows long term monitoring of metabolite induced electrical activity and voltage-dependent Ca^{+2} currents in pancreatic islet beta cells. FEBS Lett., 251 (1989), pp. 167–172

7. O. Larsson, H. Kindmark, R. Bränström, B. Fredholm, P.-O. Berggren. Oscillations in K_{ATP} channel activity promote oscillations in cytoplasmic free Ca^{+2} concentration in the pancreatic beta cell. Proc. Natl. Acad. Sci. USA, 93 (1996), pp. 5161–5165

8. P.A. Smith, F.M. Ashcroft, P. Rorsman. Simultaneous recordings of glucose dependent electrical activity and ATP-regulated K^+ currents in isolated mouse pancreatic beta cells. FEBS Lett., 261 (1990), pp. 187–190

9. Bertram R, Previte J, Sherman A, Kinard TA, Satin LS. The phantom burster model for pancreatic beta cells. Biophys J 2000; 79:2880-92; PMID: 11106596; http://dx.doi.org/10.1016/S0006-3495(00) 76525-8

10. Merrins MJ, Van Dyke AR, Mapp AK, Rizzo MA, Satin LS. Direct measurements of oscillatory glycolysis in pancreatic islet beta cells using novel fluorescence resonance energy transfer(FRET) biosensors for pyruvate kinase M2 activity. J Biol Chem 2013; 288(46):33312-22; PMID:24100037; http://dx. doi.org/10.1074/jbc.M113.508127

11. Merrins M, Fendler B, Sherman A. Metabolic oscillations in pancreatic islets depend on the intracellular Ca^{+2} level but not Ca^{+2} Oscillations. Biophys J 2010; 99:76-84; PMID:20655835; http://dx.doi. org/10.1016/j.bpj.2010.04.012

Appendix A

MATLAB Programs

The matlab codes (function files and corresponding script files) for the following models have been attached:

- Chay-Keizer single cell model
- Smolen-Keizer single cell model
- Phantom Burster single cell model
- The Dual Oscillator Model

Code for the Chay-Keizer model

```
function dydt = chaykei(t,y)
    v=y(1);
    n=y(2);
    mca=y(3);
    hca=y(4);
    ca=y(5);

    % Parameters
    cm=1;
    gca=6.5;
    gk=12;
    gl=0.04;
    gkca=0.09; % change to 0.02 to see effects of quinine/TEA
    vca=100;
    vk=-75;
    vl=-40;
    vprime=50;
    vstar=30;
    temp=20;
    r=8.9e-4;
    f=0.004;
    fara=96487;
    kdiss=1;
    kca=0.04; %change kca to 0.001 for effects of quinine

    % Gating functions
    alphamca = -0.1*((v+vprime)-25)/(exp(-((v+vprime)-25)/10)-1);
    betamca = 4*exp(-(v+vprime)/18);
    alphahca= 0.07*exp(-(v+vprime)/20);
    betahca = 1/(exp(-((v+vprime)-30)/10)+1);
    alphan = (-0.01*((v+vstar)-10)/(exp(-((v+vstar)-10)/10)-1));
    betan = (0.125*exp(-(v+vstar)/80));
    phi = 3^((temp-6.3)/10);
    % To see the effects of TEA use this
    % n_inf = alphan/(alphan+betan);
    % tau = 1/(alphan+betan);
    % taun=tau+2*tau;

    % Ionic currents:
    i_ca  = gca*mca^3*hca*(vca-v);
    i_k   = gk*n^4*(vk-v);
    i_kca = gkca*ca/(ca+kdiss)*(vk-v);
    i_l   = gl*(vl-v);

    %The differential equations
    dv = 1/cm*(2*i_ca+i_k+i_kca+i_l);
    dmca = phi*(alphamca*(1-mca)-betamca*mca);
    dhca = phi*(alphahca*(1-hca)-betahca*hca);
    dn = phi*(alphan*(1-n)-betan*n);
    % Use this dn equation for effect of TEA
    % dn = phi*(n_inf-n)/taun;
    dca = f*(3/(r*fara)*i_ca-kca*ca);

    dydt = [dv,dn,dmca,dhca,dca]';
end
-----------------------------------------------------------------------
```

```
%The script file

%Initial conditions

v0 = -54.774;
n0 = 0.00044035;
mca0 = 0.027532;
hca0 = 0.086321;
ca0 = 0.10749;

yinit = [v0,n0,mca0,hca0,ca0];
tspan = [0 50000];
options=odeset('Stats','off');

tic
[t,y] = ode15s(@chaykei,tspan,yinit,options);
toc

figure
ax1= subplot(2,1,1)
plot(t,y(:,1),'b','LineWidth',2)
title('Voltage (V)','FontSize',12)
xlabel ('Time (ms)','FontSize',12)

ax2 = subplot(2,1,2)
plot(t,y(:,5),'b','LineWidth',2)
title('[Ca^{+2}]','FontSize',12)
xlabel ('Time (ms)','FontSize',12)
```

Code for the Smolen-Keizer model

```
function dydt = smolenkeizer(t,y)
    v = y(1);
    n = y(2);
    ca = y(3);
    d = y(4);
    pc = y(5);
    pot = y(6);
    ii = y(7);
    jj = y(8);

    % Parameters
    vk = -75;
    captot = 5309;
    gcam = 1470;
    x = 0.27;
    vmj = -11;
    slopemj = 3.6;
    gcal = 6.3;
    cao = 7;
    gk = 5000;
    gatpbar = 6000;
    kone = 0.45;
    ktwo = 0.012;
    tot = 1;
    vn = -20;
    alambda = 1.2;
    slopen = 5.3;
    a = 65;
    b = 20;
    c = 60;
    fr = 0.03;
    akca = 0.12;
    rad = 7;
    farada = 96487;
    damp = 0;
    hill = 3;
    akdamp = 0.6;
    ka = 2e-05;
    % change this value to see the effects of glucose
    r = 0.76;
    r1 = 0.35;
    lambdam = 0.78;
    vm = -15;
    slopem = 6.2;
    k2s = 1.512;
    k2m = 65;
    lambdak = 1;
    k3p = 0.02;
    k3m = 0.005;
    lambdai = 1;
    vi = 36;
    slopei = 4.5;
    taui = 2600;
    lambdaj = 1;
    vj = 50;
    slopej = 6.3;
    tj = 50000;
```

```
58      tjmin = 1500;
59
60      % activation and time-constant functions
61      phicaj = 1.0/(1.0+exp((vmj-v)/slopemj));
62      phik = 1.0/(1.0+exp((vn-v)/slopen));
63      phica = 1.0/(1.0+exp((vm-v)/slopem));
64      phii = 1.0/(1.0+exp((v+vi)/slopei));
65      phij = 1.0/(1.0+exp((v+vj)/slopej));
66      alpha = 3.0e+03/(8.0e0*pi*farada*rad^3);
67      alphan = exp((v+75.0)/a);
68      betan =exp((-v-75.0)/b);
69      taun = c/(alphan+betan);
70      tauj = tjmin+tj/(exp((v+vj)/(2*slopej))
71              +exp(-(v+vj)/(2*slopej)));
72      gcab = gcam*(x*pot+(1.0-x)*phicaj*jj)+gcal;
73      ghk = cao*v/(1.0-exp(v/13.35));
74      gatp = gatpbar*(1.0+d/kone)/(1.0+d/kone+(tot-d)/ktwo);
75      k1m = lambdam*phica;
76      k1p = lambdam*(1.0-phica);
77      k2p = -k2s*ghk;
78      f2inf = k2p/(k2m+k2p);
79
80      % Ionic currents
81      ica = gcab*ghk;
82      ikv = gk*ii*n*(v-vk);
83      ikatp = gatp*(v-vk);
84
85      % The differential equations
86      dv = -(ica+ikv+ikatp)/captot;
87      dn = alambda*(phik-n)/taun;
88      dca = fr*(-alpha*ica-akca*ca-damp*ca^hill
89              /(akdamp^hill+ca^hill));
90      dd = ka*((tot-d)-d*exp(r*(1.0-(ca/r1))));
91       dpc = k1p*pot*(1.0-f2inf)-k1m*pc;
92      dpot = -(k1p*pot*(1.0-f2inf)-k1m*pc)-
93              lambdak*(k3p*f2inf*pot-k3m*(1.0-pot-pc));
94      dii = lambdai*(phii-ii)/taui;
95      djj = lambdaj*(phij-jj)/tauj;
96      dydt =[dv,dn,dca,dd,dpc,dpot,dii,djj]';
97  end
98  ------------------------------------------------------------------
99  %The script file
100
101   % Initial conditions
102 v0=-53;
103 n0=0.002;
104 ca0=0.15;
105 d0=0.42;
106 pc0=0.9;
107 pot0=0.02;
108 ii0=0.98;
109 jj0=0.47;
110
111 yinit = [v0,n0,ca0,d0,pc0,pot0,ii0,jj0];
112 tspan = [0 50000];
113 options=odeset('Stats','off');
114
```

```
115 tic
116 [t,y] = ode15s(@smolenkeizer,tspan,yinit,options);
117 toc
118
119 figure
120 ax1 = subplot(2,1,1)
121 plot(t,y(:,1),'b','LineWidth',2)
122 title('Voltage (mV)','FontSize',20);
123 set(gca,'FontSize',17) % xlabel('Time (ms)');
124
125 ax2 = subplot(2,1,2)
126 plot(t,y(:,3),'b','LineWidth',2)
127 title('[Ca^{+2}]','FontSize',20);
128 xlabel('Time (ms)','FontSize',20);
129 set(gca,'FontSize',17)
```

Code for the Phantom Burster model

```
% Phantom bursting model, with 2 fast and 2 slow variables.
% Units: V = mV; t = ms; g = pS; I = fA

function dydt = phantomburster(t,y)
    v = y(1);
    n = y(2);
    s1 = y(3);
    s2 = y(4);

    % Parameters
    vl = -40;
    vca = 100;
    vk = -80;
    lambda = 1.1;
    gca = 280;
    gk = 1300;
    gl = 25;
    vs1 = -40;
    taus1 = 1000; %could go upto 10s
    vs2 = -42;
    taus2 = 120000; %could be as small as 1min
    gs2 = 32;
    gs1 = 3; % for slow bursting
    % gs1 = 4; %for medium bursting 'phantom bursting'
    % gs1 = 20; % for fast bursting
    cm = 4524;
    tnbar = 9.09;
    vm = -22;
    vn = -9;
    sm = 7.5;
    sn = 10;
    ss1 = 0.5;
    ss2 = 0.4;

    % activation and time-constant functions
    minf = 1.0/(1.0+exp((vm-v)/sm));
    ninf = 1.0/(1.0+exp((vn-v)/sn));
    taun = tnbar/(1.0+exp((v-vn)/sn));
    s1inf = 1.0/(1.0+exp((vs1-v)/ss1));
    s2inf = 1.0/(1.0+exp((vs2-v)/ss2));

    % Ionic currents
    ica = gca*minf*(v-vca);
    ik = gk*n*(v-vk);
    il = gl*(v-vl);
    is1 = gs1*s1*(v-vk);
    is2 = gs2*s2*(v-vk);

    % The differential equations

    if 15000<t && t<45000
        istim = 0;
    else
        istim=0;
    end

    dv = -( ica + ik + il + is1 + is2 )/cm - istim/cm;
```

```
    dn = lambda*(ninf - n)/taun;
    ds1 = (s1inf - s1)/taus1;
    ds2 = (s2inf - s2)/taus2;

    dydt = [dv, dn, ds1, ds2]';
end
-----------------------------------------------------------------------
% The script file

 % Initial conditions

v0 = -43.0;
n0 = 0.03;
s10 = 0.1;
s20 = 0.434;

yinit = [v0,n0,s10,s20];
tspan = [0 100000];
options=odeset('Stats','off');

tic
[t,y] = ode15s(@phantomburster,tspan,yinit,options);
toc

figure(1);
% t(t<3e4) = NaN;
plot(t,y(:,1),'b','LineWidth',2)
title('Fast bursting - Voltage (mV)' ,'Fontsize',21)
xlabel('Time (ms)' ,'Fontsize',21);
set(gca,'FontSize',25)
```

Code for the Dual Oscillator Model

```
% Program for a beta-cell model coupled to glycolysis -DOM
% This was published by Bertram, Sherman et. al.
% Biophysical Journal, 87:3074-3087, Nov. 2004.

% State variables: % V    -- membrane potential
% n    -- activation of delayed rectifier
% Ca   -- free cytosolic calcium concentration
% ADP  -- cytosolic ADP concentration
% CaER -- concentration of free calcium in the ER
% G6P  -- glucose 6-phosphate concentration
% FBP  -- fructose 1,6-bisphosphate concentration

function dydt = dualoscillator(t,y)

    % y = [V, n, Ca, CaER, ADP, G6P, FBP];
    V = y(1);
    n = y(2);
    Ca = y(3);
    CaER = y(4);
    ADP = y(5);
    G6P = y(6);
    FBP = y(7);

    % Parameter sets for various behaviors:
    % k_gamma = 10 for all of the sets!
    % Note: An inc. in R_GK is like an inc in gluc.

    % for compund bursting
    % R_GK = 0.2; gKATPbar = 25000; gKCabar = 600;

    % for slow bursting
    % R_GK = 0.2; gKATPbar = 27000; gKCabar = 100;

    % for subthreshold bursting
    % R_GK = 0.2; gKATPbar = 30000; gKCabar = 100;

    % for accordian bursting
    %R_GK = 0.2; gKATPbar = 23000; gKCabar = 600;

    % for fast bursting
    % R_GK = 0.4; gKATPbar = 25000; gKCabar = 600;

    % ------------------------------------------------------------
    % Channel properties

    Cm = 5300;
    VK = -75;
    gK = 2700;
    taun = 20;
    ninf = 1/(1+exp(-(16+V)/5));
    gCa = 1000;
    VCa = 25;
    minf = 1/(1+exp(-(20+V)/12));
    % gKCabar = 600; (uncomment out one of the sets!)
    Kd = 0.5;

    % Ionic currents:
```

```
58      IK = gK*n*(V-VK);
59      ICa = gCa*minf*(V-VCa);
60      gKCa = gKCabar/(1+(Kd/Ca)^2);
61      IKCa = gKCa*(V-VK);
62
63      % IKATP (see below, after calc. of nucleotide concs.)
64      % gKATPbar = 25000;(uncomment out one of the sets!)
65
66      % Calcium Handling
67      alpha = 4.50e-6;
68      kPMCA = 0.2;
69      fcyt = 0.01;
70      fer = 0.01;
71      % sigmav=cyt volume/ER volume = V_cyt/V_er
72      sigmav = 31;    pleak = 0.0002;
73      kSERCA = 0.4;
74      Jmem = -(alpha*ICa + kPMCA*Ca);
75      JSERCA = kSERCA*Ca;
76      Jleak = pleak*(CaER - Ca);
77      Jer = Jleak - JSERCA;
78
79      % ---------------------------------------------------------------
80      % Glycolytic and Keizer-Magnus components
81      % Parameters
82      % R_GK--glucokinase rate
83      % Atot--total adenine nucleotide concentration (micromolar)
84      % K1--Kd for AMP binding
85      % K2--Kd for FBP binding
86      % K3--Kd for F6P binding
87      % K4--Kd for ATP binding
88      % famp, etc--Kd amplification factors for heterotropic binding
89      % famp corresponds to f13 in the paper
90      % fmt  corresponds to f41 in the paper
91      % ffbp corresponds to f23 in the paper
92      % fbt  corresponds to f42 in the paper
93      % fatp corresponds to f43 in the paper
94      % R_GPDH--glyceraldehyde phosphate dehydrogenase rate
95
96      % Glycolytic parameters
97      K1 = 30;
98      K2 = 1;
99      K3 = 50000;
100     K4 = 1000;
101     famp = 0.02;
102     fmt = 20;
103     ffbp = 0.2;
104     fbt = 20;
105     fatp = 20;
106
107     % Glycolytic expressions
108     F6P = 0.3*G6P;
109     % nucleotide concentrations used for R_PFK
110     Atot = 3000;
111     rad = sqrt((ADP-Atot)^2-4*ADP^2);
112     ATP = 0.5*(Atot-ADP+rad);
113     % Use this to see how the glyc. comp. osc. independently!
114     % ATP = 2000;
```

```
115       AMP = ADP^2/ATP;
116
117       % Iterative calculation of R_PFK
118       %(cf. Smolen95, Eq. 12)
119       % alpha = 1 -- AMP bound
120       % beta = 1 -- FBP bound
121       % gamma = 1 -- F6P bound
122       % Δ = 1 -- ATP bound
123       % (alpha,beta,gamma,Δ)
124
125       % (0,0,0,0)
126       weight1 = 1;
127       topa1 = 0;
128       bottom1 = weight1;
129
130       % (0,0,0,1)
131       weight2 = ATP^2/K4;
132       topa2 = topa1;
133       bottom2 = bottom1+weight2;
134
135       % (0,0,1,0)
136       weight3 = F6P^2/K3;
137       topa3 = topa2+weight3;
138       bottom3 = bottom2+weight3;
139
140       % (0,0,1,1)
141       weight4 = (F6P*ATP)^2/(fatp*K3*K4);
142       topa4 = topa3+weight4;
143       bottom4 = bottom3+weight4;
144
145       % (0,1,0,0)
146       weight5 = FBP/K2;
147       topa5 = topa4;
148       bottom5 = bottom4+weight5;
149
150       % (0,1,0,1)
151       weight6 = (FBP*ATP^2)/(K2*K4*fbt);
152       topa6 = topa5;
153       bottom6 = bottom5+weight6;
154
155       % (0,1,1,0)
156       weight7 = (FBP*F6P^2)/(K2*K3*ffbp);
157       topa7 = topa6+weight7;
158       bottom7 = bottom6+weight7;
159
160       % (0,1,1,1)
161       weight8 = (FBP*F6P^2*ATP^2)/(K2*K3*K4*ffbp*fbt*fatp);
162       topa8 = topa7+weight8;
163       bottom8 = bottom7+weight8;
164
165       % (1,0,0,0)
166       weight9 = AMP/K1;
167       topa9 = topa8;
168       bottom9 = bottom8+weight9;
169
170       % (1,0,0,1)
171       weight10 = (AMP*ATP^2)/(K1*K4*fmt);
```

```
172       topa10 = topa9;
173       bottom10 = bottom9+weight10;
174
175       % (1,0,1,0)
176       weight11 = (AMP*F6P^2)/(K1*K3*famp);
177       topa11 = topa10+weight11;
178       bottom11 = bottom10+weight11;
179
180       % (1,0,1,1)
181       weight12 = (AMP*F6P^2*ATP^2)/(K1*K3*K4*famp*fmt*fatp);
182       topa12 = topa11+weight12;
183       bottom12 = bottom11+weight12;
184
185       % (1,1,0,0)
186       weight13 = (AMP*FBP)/(K1*K2);
187       topa13 = topa12;
188       bottom13 = bottom12+weight13;
189
190       % (1,1,0,1)
191       weight14 = (AMP*FBP*ATP^2)/(K1*K2*K4*fbt*fmt);
192       topa14 = topa13;
193       bottom14 = bottom13+weight14;
194
195       % (1,1,1,0) -- the most active state of the enzyme
196       weight15 = (AMP*FBP*F6P^2)/(K1*K2*K3*ffbp*famp);
197       topa15 = topa14;
198       topb = weight15;
199       bottom15 = bottom14+weight15;
200
201       % (1,1,1,1)
202       weight16 = ...
              (AMP*FBP*F6P^2*ATP^2)/(K1*K2*K3*K4*ffbp*famp*fbt*fmt*fatp);
203       topa16 = topa15+weight16;
204       bottom16 = bottom15+weight16;
205
206       % Phosphofructokinase rate
207       % lambda, Vmax as in Smolen95, Eq. 3
208       lambda = 0.06; %in the paper lambda <<1
209       Vmax = 2;
210       R_PFK = Vmax*(lambda*topa16 + topb)/bottom16;
211       % GPDH flux:
212       R_GPDH = 0.2*sqrt(FBP);
213
214       % KATP channel
215       Kdd = 17;
216       Ktd = 26;
217       Ktt = 1;
218
219       % KATP channel open probability
220       %(reference: Magnus and Keizer (1998))
221       mgADP = 0.165*ADP;
222       ADP3m = 0.135*ADP;
223       ATP4m = 0.05*ATP;
224       topo = 0.08*(1+2*mgADP/Kdd) + 0.89*(mgADP/Kdd)^2;
225       bottomo = (1+mgADP/Kdd)^2 * (1+ADP3m/Ktd+ATP4m/Ktt);
226       oinf = topo/bottomo;    gKATP = gKATPbar*oinf;
227       IKATP = gKATP*(V-VK);
```

```
228
229     % glycolytic input to mitochondrial ADP equation:
230     k_gamma = 10;
231     v_gamma = 2.2;
232     gamma = v_gamma*(R_GPDH/(k_gamma+R_GPDH));
233     r = 1;
234     taua = 300000;
235     r1 = 0.35;
236
237     % conversion parameter for glycolytic subsystem
238     % kappa erroneously called lambda in paper;
239     % renamed kappa for consistency with Smolen,
240     %JTB, 1995 and Pedersen et al, 2005.
241     kappa = 0.005;
242     % R_GK = 0.2; (uncomment out one of the sets!)
243
244     % Differential equations
245
246     dV = -(IK + ICa + IKCa + IKATP)/Cm;
247     dn = (ninf-n)/taun;
248     dCa = fcyt*(Jmem + Jer);
249     dCaER = -fer*sigmav*Jer;
250     dADP = (ATP-ADP*exp((r + gamma)*(1-Ca/r1)))/taua;
251     dG6P = kappa*(R_GK - R_PFK);
252     dFBP = kappa*(R_PFK - 0.5*R_GPDH);
253
254     dydt = [dV, dn, dCa, dCaER, dADP, dG6P, dFBP]';
255 end
256 ---------------------------------------------------------------------
257 %The script file
258
259 % Initial conditions:
260
261 V0 = -60;
262 n0 = 0;
263 Ca0 = 0.1;
264 CaER0 = 185;
265 ADP0 = 780;
266 G6P0 = 200;
267 FBP0 = 40;
268
269 yinit = [V0,n0,Ca0,CaER0,ADP0,G6P0,FBP0];
270 tspan = [0 1000000];
271 options=odeset('Stats','off');
272
273 tic
274 [t,y] = ode15s(@dualoscillator,tspan,yinit,options);
275 toc
276
277 % figure
278 % plot(t,y(:,1),'b','LineWidth',2)
```